ELECTRON–ELECTRON INTERACTIONS IN A TWO DIMENSIONAL QUANTUM DOT

A THESIS SUBMITTED TO
THE GRADUATE SCHOOL OF NATURAL AND APPLIED SCIENCES
OF
THE MIDDLE EAST TECHNICAL UNIVERSITY

BY

NURTEN AKMAN

IN PARTIAL FULFILLMENT OF THE REQUIREMENTS FOR THE DEGREE OF

DOCTOR OF PHILOSOPHY

IN

THE DEPARTMENT OF PHYSICS

SEPTEMBER 1999

Approval of the Graduate School of Natural and Applied Sciences.

Prof. Dr. Tayfur Öztürk
Director

I certify that this thesis satisfies all the requirements as a thesis for the degree of Doctor of Philosophy.

Prof. Dr. Sinan Bilikmen
Head of Department

This is to certify that we have read this thesis and that in our opinion it is fully adequate, in scope and quality, as a thesis for the degree of Doctor of Philosophy.

Prof. Dr. Mehmet Tomak
Supervisor

Examining Committee Members

Prof. Dr. Mehmet Tomak

Prof. Dr. Bilal Tanatar

Prof. Dr. Çiğdem Erçelebi

Assoc. Prof. Dr. Hatice Kökten

Dr. Sadi Turgut

ABSTRACT

ELECTRON–ELECTRON INTERACTIONS IN A TWO DIMENSIONAL QUANTUM DOT

Akman, Nurten

Ph.D., Department of Physics

Supervisor: Prof. Dr. Mehmet Tomak

September 1999, 67 pages.

Quantum dots, being zero dimensional structures, are extremely interesting low-dimensional systems. They can be thought of as artificial atoms where the experimentally created confining potential replaces the potential of the nucleus. The number of electrons confined within these artificial atoms typically varies between 2 and 200 which is comparable with that of natural atoms. In quantum dots, or artificial atoms, the Coulomb interaction between the electrons is extremely important for understanding their quantum mechanical properties. Hence the overall discussion of these interaction effects, playing an important role in the energy spectrum and in the distributions of few-electrons in a 2D circular quantum dot, is presented in this work. The type of confining potential is the hard-wall which is the most commonly used confining potential model together with the parabolic one. For the analysis of the energy spectrum, first the total Hamiltonian is expressed in the dimensionless form, and then transformed into the second quantization language. By taking into account the circular geometry of the dot, and the spin independence of the Coulombic interaction, the good quantum numbers are identified to be the total spin, and the z- components of

the total spin and the total orbital angular momentum. Pertinent to the few–electron case only 2, 3 and 4 electrons are considered and their ground state energy eigenvalues are calculated as a function of the dimensionless coupling constant λ. Here λ measures the dot radius in units of the effective Bohr radii and controls the transition from the atomic regime to the Wigner molecular regime. For the numerical analysis of the energy spectrum, an exact diagonalization method is used and the total Hamiltonian is diagonalized for given values of the good quantum numbers. In the remaining part of the work, the charge density and the pair correlation function are calculated for three spin-polarized interacting electrons in the 2D circular quantum dot. Variation of the charge density with radial distance as well as that of the pair correlation function with azimuthal angle together with their size dependence show clearly the atomic limit and the formation of the Wigner molecule.

Keywords: Low-dimensional systems, quantum dot, charge density, pair correlation function, electron-electron interactions, exact diagonalization method, Wigner molecule.

ÖZ

İKİ BOYUTLU KUVANTUM NOKTASINDAKİ ELEKTRON–ELEKTRON ETKİLEŞİMLERİ

Akman, Nurten

Doktora , Fizik Bölümü

Tez Yöneticisi: Prof. Dr. Mehmet Tomak

Eylül 1999, 67 sayfa.

Kuvantum noktaları, sıfır boyutlu yapılar olarak son derece ilginç düşük boyutlu sistemlerdir. Bu yapılar, doğal atomlardaki çekirdek potansiyelinin yerini yapay bir potansiyelin alması nedeniyle yapay atomlar olarak da düşünülebilirler. Bu tür yapılarda doğal atomlardakiyle kıyaslanabilen elektron sayısı tipik olarak 2 ila 200 arasında değişmektedir. Kuvantum noktalarında, diğer bir deyimle yapay atomlarda, elektronlar arasındaki Coulomb etkileşmesi, onların kuvantum mekaniksel özelliklerini anlamak için son derece önemlidir. Bu nedenle elektronların enerji tayfında ve iki boyutlu dairesel bir kuvantum noktasındaki dağılımında önemli rol oynayan bu etkileşimlerin ayrıntılı tartışması tezde sunulmaktadır. Hapsetme potansiyelinin tipi parabolik potansiyelle birlikte en çok kullanılan sonsuz potansiyel engelidir. Toplam Hamiltoniyen, enerji tayfının analizi için öncelikle boyutsuz olarak ifade edilmiş ve daha sonra ikinci kuvantlama diline dönüştürülmüştür. Kuvantum noktasının dairesel yapısı ve Coulomb etkileşiminin spinden bağımsız oluşu dikkate alınarak, toplam spin ile toplam spin ve toplam yörüngesel açısal momentin z bileşenleri uygun kuvantum sayıları olarak belirlenmiştir. Bir kaç elektron durumuna uygun olarak sadece 2, 3, ve 4 elektron

çalışılmış ve onların en düşük enerji özdeğerleri boyutsuz bağlaç sabiti λ cinsinden hesap edilmiştir. Bu çalışmada λ, noktanın yarıçapını etkin Bohr yarıçap biriminde ölçmekte ve atomik rejimden Wigner molekülsel rejime olan geçişi kontrol etmektedir. Enerji tayfının sayısal analizi için tam köşegenleştirme metodu kullanılmış ve toplam Hamiltoniyen uygun kuvantum sayılarının verilen değerleri için köşegenleştirilmiştir. Tezin geri kalan bölümünde ise iki boyutlu dairesel kuvantum noktasında etkileşen spin kutuplu üç elektron için yük yoğunluğu ve çift korelasyon fonksiyonu hesaplanmıştır. Yük yoğunluğunun radyal mesafe ile, çift korelasyon fonksiyonunun ise açı ile değişimi ve de her ikisinin kuvantum noktasının büyüklüğüne olan bağlılığı açık bir şekilde atomik limiti ve Wigner molekülünün oluşumunu göstermiştir.

Anahtar Sözcükler: Düşük-boyutlu sistemler, kuvantum noktası, yük yoğunluğu, çift korelasyon fonksiyonu, elektron-elektron etkileşimleri, tam köşegenleştirme metodu, Wigner molekülü.

ACKNOWLEDGMENTS

I would like to express my sincere appreciation to my supervisor, Prof. Mehmet Tomak for his guidance and invaluable help throughout my Ph.D. research.

Secondly, I would like to thank to three young scientists, Dr. Durmuş Ali Demir, Dr. Ceyhun Bulutay and Dr. Sadi Turgut for their scientific advices and friendly attitude.

I am thankful to my friends, Şanver Narin and Haldun Çamurtaş for their computational help. I would like to also thank Murat Taş for his friendly personality.

Finally, I am deeply grateful to my family for their support and encouragement throughout my whole education.

TABLE OF CONTENTS

LIST OF FIGURES

CHAPTER 1

INTRODUCTION

In the late 70's a new research field of the condensed matter physics has started after understanding the fact that the size of a conductor, if it is made small enough, is very crucial in determining its electronic properties. In the following two decades rapid progress in crystal growth techniques has made it possible to realize semiconductor microstructures which are so small that their electronic and optical properties are different from those of bulk materials. Various theoretical and experimental discoveries have proven that when the system size approaches the size of the electronic wavelength, quantum effects manifest themselves in their properties. After these developments, the name "mesoscopic physics" has been coined to describe this new research field since microstructures (or submicron-size systems) are larger than the natural atoms and smaller than the macroscopic samples. Their typical dimensions range from nanometers to a few microns, and their size and shape can be precisely controlled with the advanced nanofabrication technology.

The well-known examples of mesoscopic structures are quantum wells ($\lambda_F \sim L_x < L_y < L_z$: quasi 2D (thin films) and $L_x < \lambda_F << L_y < L_z$: 2D (MOSFETs, heterostructures)), where the electrons are confined in one spatial direction. The

translational motion of electrons in the plane perpendicular to the confinement direction is not restricted. On the other hand, if the electrons are confined in two space dimensions and free to move only in one direction ($L_x < L_y \sim \lambda_F << L_z$: quasi 1D (quantum wires) and $L_x < L_y < \lambda_F << L_z$: 1D) then such mesoscopic structures are called quantum wires. The ultimate example in this area is a quantum dot where the confinement of electrons exists in all three spatial directions ($L_x < L_y < L_z < \lambda_F$: 0D (quantum dots)).

Mesoscopic structures enable us to probe the properties of the solid state through the energy and the length scales which are not normally accessible to present–day devices. The most important length scales characterizing the mesoscopic systems are the phase coherence length and the mean free path. The phase coherence length is defined as the average distance covered by an electron before losing its phase memory by an inelastic collision. Typically it ranges from 0.1 to 1 μm and is the relevant length scale for the quantum interference transistors. The average distance traveled by an electron before suffering an elastic collision is known as the mean free path. It can exceed 10 μm in the 2DEG of a modulation doped GaAs/AlGaAs heterojunction which can be used in the ballistic transmission devices (another type of mesoscopic device), where the information is carried by beams of ballistic electrons.

The third type of the mesoscopic devices is the resonant tunneling quantum dot devices at which electron tunneling has a vital role as happens in current day devices (especially the Esaki tunnel diode and the hot electron transistor). The tunneling area in the mesoscopic devices is less than 1 μm^2 and this increases the

energy of the electron states and also modifies the current-voltage characteristics of the resonant tunneling.

The single electron transistors (SETs) based on the Coulomb blockade are the most attractive types of all the mesoscopic devices. The relevant energy scale is the charging energy, $e^2/2C$. If the capacitance can be made small enough then $e^2/2C$ can become much larger than the thermal energy, kT, and applied bias, eV. As a result, the current cannot flow through the transistor until the applied bias eV exceeds the charging energy. The SETs with dimensions less than 0.1 μm are now possible, but, unfortunately, they operate at the liquid helium temperature. In the future, if the technology lets the researchers to make devices with dimensions less than 0.01 μm, they can operate at room temperature and one may find application of SETs in our daily life.

1.1 Formation of Quantum Dots

Fabrication of the low dimensional semiconductors began in the early 70's, when the first two dimensional quantum wells were successfully manufactured by the thin-film epitaxial techniques. By the well controlled epitaxial growth techniques like molecular beam epitaxy (MBE) and metal organic chemical vapor deposition (MOCVD), it is now possible to grow two dimensional ultrahigh purity thin films of compound semiconductors, where the thickness of each layer can be precisely controlled down to a single layer of atoms ($\sim$ a few $\mathring{A}$ thick). Quantum wells have now formed the basis of many devices such as laser diodes found in compact-disc players, sensitive microwave receivers that pull in signals from a

satellite dish, and laser sources for fiber optic communications. In addition to the quantum wells, researchers have also managed to confine electrons in three spatial directions.

The first zero dimensional quantum confinement was realized in the early 80's by noticing unusual optical spectra from samples of glass containing the semiconductors cadmium sulfide or cadmium selenide [1-6]. The samples are prepared by high temperature precipitation of semiconductors in molten silicate glass matrices. After melting, the desired semiconductor components are added into the glasses. Then a rapid cooling process of the melt is followed by a secondary heat treatment which means annealing between 400 and 700 $^{\circ}C$. During the annealing process, semiconductor crystallites precipitate in the glass matrices. The average radius of the crystallites which ranges from tens to thousands of angstroms is determined by choosing the proper annealing conditions (temperature and time). The quantum size effect in these crystallites is revealed as a shift to shorter wavelengths of the absorption spectra with the decrease of crystallite size. This effect can be seen clearly in cadmium selenide clusters by progression from deep red to orange and yellow as the diameter of the cadmium selenide cluster is reduced.

In addition to the growth of quantum dots inside a glass matrix, colloidal suspensions of nanocrystallites by chemical precipitation from solutions is the second commonly used technique [7-10]. The quantum dots grow in tiny droplets of cadmium solution wrapped in soap-like compounds. The cadmium droplets are suspended in a bath of a selenium containing solution. As selenium ions migrate into the droplets, clusters of semiconducting compound cadmium selenide

gradually precipitate. The researchers could control the size of the precipitate in a range between 15 and about 500 $\mathring{A}$. As is seen in the glass encased nanocrystallites, as the crystallite size is decreased, the fundamental absorption energy corresponding to the minimum excitation moves to shorter wavelengths (higher energies). This produces discrete electronic states in the valence and conduction band of the colloidal semiconductor, proving the quantum confinement, and increases its effective band gap. The blueshift in the absorption threshold is a consequence of the increased gap between the highest occupied and the lowest unoccupied states.

Very small colloidal semiconductor particles have been extensively studied due to their potential applications in the area of solar energy conversion and photocatalysis. Also they enable us to study the transition from molecular to bulk semiconductor properties. In addition to the II-VI compounds like sulfides and selenides of Cd, Zn, Pb and CuCl, the chemical precipitation of III-V compounds such as InP has also been realized [11]. When compared with the growth of quantum dots in glass matrices, it has basically similar advantages and problems, but it proposes the possibility of manipulating the crystallite after the original growth [12].

Another excessively used technique in this area is the formation of small semiconductor clusters inside the nanometer-scale cavities of zeolites. It is possible to form smaller and more uniform semiconductor clusters than is possible with colloids. Moreover, the optical properties of small semiconductor clusters can depend not only on the size but also on the state of aggregation. The zeolites

provide better media than the colloidal solution for controlling the aggregation. And it is also possible to build a superlattice structure by filling up the zeolite cavities. In Ref. [13], the optical properties of CdS and PbS clusters encapsulated in the zeolites have been reported with a dramatic deviation from their bulk optical properties. At low concentration of CdS in the zeolite, isolated clusters with size < 13 $\AA$ were obtained showing an absorption peak around 280 nm. Clusters of this size have properties which approach the molecular properties in nature. At higher concentrations of CdS, individual clusters aggregated into a three dimensionally grown superlattice. The absorption threshold shifts to 420 nm (still quite lower than the bulk value of 540 nm) and an exciton like feature evolves at 350 nm proving their solid state behavior. Thus, as it happens in colloids, the zeolite encapsulation provides a way to study semiconductor clusters in both their molecular and solid state limits.

Even though various growth techniques have been developed to encase nanocrystals inside another material, none of them could have been able to overcome certain problems appearing in the optical measurements. The uncertainity of the dot size distribution is the most striking problem that leads to pronounced inhomogeneous broadening in the optical spectra. In addition to the inhomogeneous broadening, one has to deal with homogeneous broadening of the optical resonances resulting from the scattering of the optically generated charge carriers inside the dot with imperfections, impurities or phonons.

Another obvious way to make quantum dots is to start with an ordinary quantum well, pattern it lithographically with electron beams, and carve it up

with a beam of ions. The first lithographic quantum dots have been made in 1987 by cutting slabs of quantum well material into pillars by means of advanced etching techniques [14,15].

They used the electron beam lithography to make pillars 100 $\AA$ wide. In the first step of fabrication, an electron beam scans the surface of a semiconductor containing a buried layer of quantum well material. The semiconductor surface has been coated with a thin polymer layer, a resist, which was removed at places where the electron beam was scanned at high intensity. A metal layer is deposited in the resulting area, and then a solvent removes the remaining resist leaving only a thin layer of metal on the surface of semiconductor. Reactive ions then etch away the structure except where it is protected by metal, leaving a quantum dot (a pillar) behind. All of these steps are schematically shown in Fig. 1.1. If the diameter of the pillar can be made very small, then one can observe the harmonic series of peaks that indicates quantum confinement in the current-voltage spectrum. In contrast to the nanocrystallite formation, this technique makes it possible to grow a single quantum dot that is isolated from its environment and study its properties. Moreover, the lithographic fabrication method naturally protects the quantum dot from damaging surface effects which produce trouble in nanocrystallites. The top and the bottom faces of the quantum dot are single crystal interfaces made by molecular beam epitaxy and are essentially perfect.

Subsequently, the researchers could make quantum dots by placing tiny gate electrodes on top of a buried layer that confines electrons in a two dimensional plane. They could manage to eliminate surface effects entirely with this method

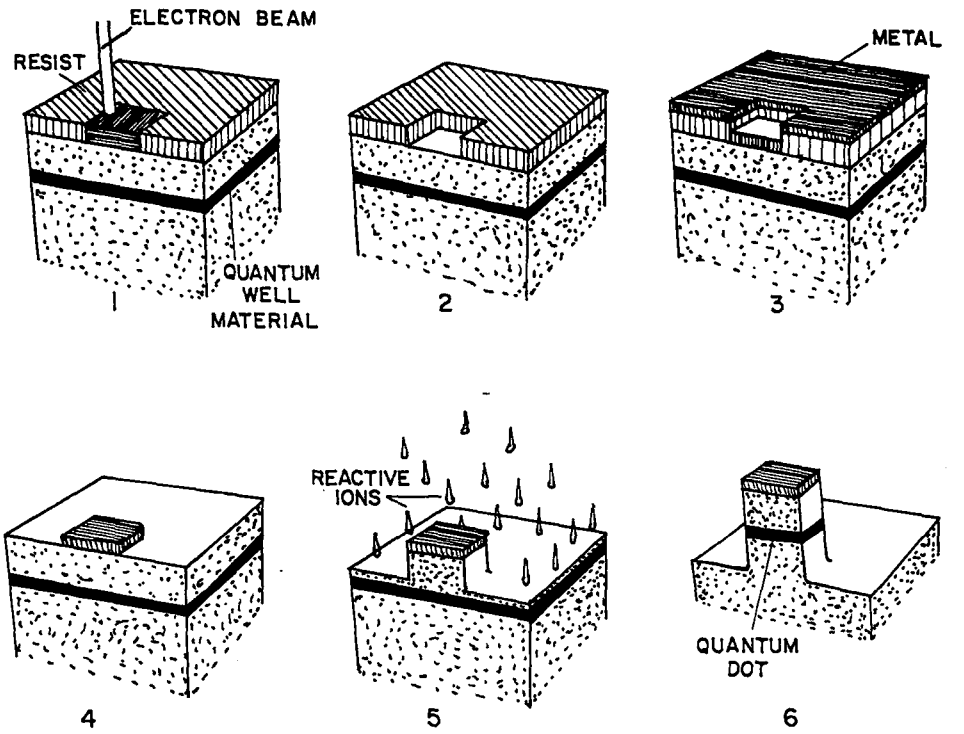

Figure 1.1: Quantum dot formation by using the electron–beam lithography.

and put as many or as few electrons in the dot by varying the gate voltage. Due to the ability of changing the number of electrons in the dot as desired, quantum dots are also named as artificial atoms. In natural atoms, confinement of the electrons is caused by the radially directed electrostatic force of the nucleus, and the electron wave functions are radially symmetric. In these artificial atoms, the shape of the gate electrodes controls the size, shape and symmetry of the confining potential. This enables us to study the electrons confined in square or rectangular atoms which are previously inaccessible in nature. A schematic diagram of one such structure forming an artificial atom or quantum dot is given in Fig. 1.2.

The structure mainly consists of a heterojunction between two semiconductors

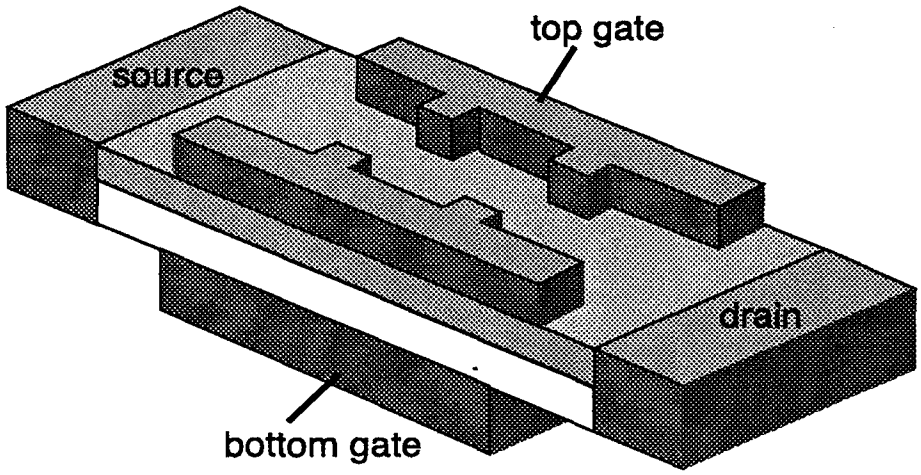

Figure 1.2: A three–dimensional view of the electrode geometry which is lithographically patterned on the surface to form a quantum dot structure.

(such as GaAs and AlGaAs), top and bottom gate, and source and drain contacts [16]. The wider gap semiconductor (AlGaAs) is doped with donors and the electrons migrate to the narrower gap semiconductor (GaAs) where they form a quasi two–dimensional electron sheet (2DES) at the heterojunction interface. The top gate (or Schottky electrodes) is lithographically patterned on the surface and its geometry is shown from a top view in Fig. 1.3. When a negative bias is applied to the surface metallic electrode, the electrons beneath it in the 2DES are repelled, and without the four stubs (narrow constrictions) on the top gate, two adjacent electrodes with a narrow gap between them (W_o is between 400 and 600 nm) convert the 2DES into a quasi one-dimensional wire. The four stubs patterned in this narrow gap which are typically 250 nm wide and 100 nm long create two dimensional barriers for electrons along the narrow electronic channel, converting the quasi one-dimensional wire into a quantum dot.

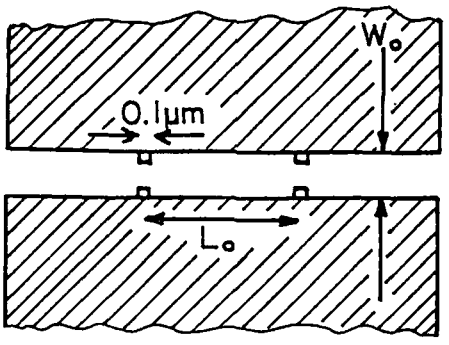

Figure 1.3: Top view of the electrode geometry in Fig. 1.2. Typically $L_0 \approx 0.6 - 1\mu m$ and $W_0 \approx 0.4 - 0.6\mu m$.

Electrostatic confinement by split-gate geometry is another common technique to realize the quantum dot structures [17,18]. Fig. 1.4 shows a schematic layout of the geometry which is fabricated on top of a GaAs/AlGaAs heterostructure containing a two dimensional electron gas. Gate F in this figure is named as the finger gate, gates 1 to 4 as the quantum point contact (QPC) gates, and gate C as the center gate. When the QPC gates 3 and 4 are held at zero potential, applying a negative voltage to the gates F, 1, 2 and C forms a quantum dot in the 2DEG. QPC gates 1 and 2 are used to control the conductance of the tunnel barriers between the quantum dot and the wide 2DEG regions, and center gate C is used to vary the number of electrons in the quantum dot. This type of gate geometry also allows to define a single QPC in the 2DEG by applying only a negative voltage to the finger gate and to one of the QPC gates, while keeping zero voltage at the other gates. Thus, one can measure the conductances of the individual QPCs and compare them to the conductance of the quantum dot.

Moreover, the split gate technique enables to form an artificial one-dimensional crystal, which consists of a sequence of quantum dots, coupled by point contacts

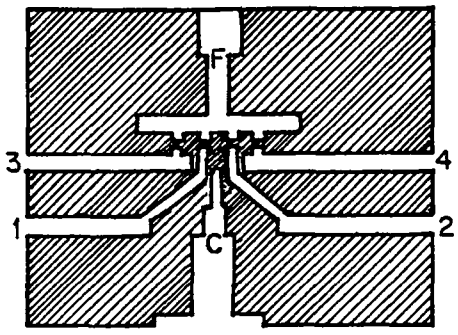

Figure 1.4: Scanning Electron Micrograph of the split gate geometry. The distance between gate F and C is 1 μm and between two adjacent QPCs is 0.8 μm.

[19,20]. Just as a single quantum dot displays energy levels analogous to those of a natural atom, an artificial lattice has an energy band structure analogous to that of a crystalline semiconductor. The formation of the energy band structure which is one of the basic principles of solid state theory has been clearly observed in conductance measurements of the 1D artificial crystal at a fixed magnetic field [19,20].

The formation of the quantum dot structures by encasing them inside another material or by advanced lithographic techniques suffers from the surface effects, process induced damage and rough heterostructure interfaces. A promising technique for the clean and damage–free formation of quantum dot structures directly on the epilayer surface is the layer–then–island growth mode (Stranski-Krastanow) in lattice mismatched systems. First, a two dimensional layer is deposited on the substrate material as schematically shown in Fig. 1.5. After a critical layer deposition thickness is obtained, the surface converts to three dimensional highly strained dot structures grown on the heterostructure interface.

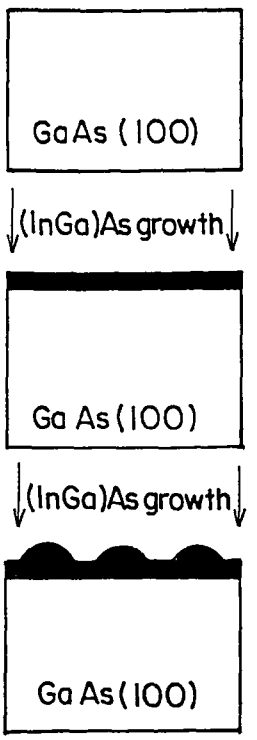

Figure 1.5: Schematic diagram of the formation of quantum dots in the Stranski–Krastanow growth mode.

The resulting quantum dots fulfill the size requirements and maintain good uniformity in the ensemble of the dots. Among the various combinations of III-V semiconductors based on P [21-24] or Sb [25-27] compounds, and Si-SiGe alloys [28-30], the strained InGaAs/GaAs structure has been most widely studied [31-35] for the experimental realization of the spontaneously formed islands due to the large lattice mismatch (7 %) between GaAs and InAs.

InGaAs quantum dots on GaAs by molecular beam epitaxy (MBE) [33] and by metalorganic chemical vapor deposition (MOCVD) [34], and InP quantum dots on an InGaP/GaAs substrate by hydride vapor phase epitaxy (VPE) [22] and by MOCVD [23] were successfully produced. But only the MBE and MOCVD growth techniques realized the quantum dot sizes smaller than 50 nm. Dot sizes

ranging from about 18 nm up to more than 50 nm have been obtained by the MBE growth technique. However, by the MOCVD growth technique, highly uniform strained InGaAs quantum dots with a diameter of about 15 nm could be observed in SEM micrographs. Furthermore, strong and sharp photoluminesence emission spectra of these quantum dots also proved uniform dots with negligible size fluctuations and a homogeneous heterostructure interface. The average dot size and areal dot density could be controlled linearly by growth temperature and InGaAs deposition thickness. Thus, since the Stranski-Krastanow growth technique does not require nanolithography and etching or implantation induced process, the dots are grown in situ without breaking the growth run, resulting in a homogeneous surface morphology and avoiding defect creation.

In conclusion, various growth techniques have been developed to form quantum dot structures during the last two decades. The most challenging problem in the quantum dot formation is to obtain essentially perfect control over the dot size and purity of these very small structures. The quantum dots made by "top-down" approach (carving by electron beam lithography or sequeezing semiconductors by metallic gates) need to be further improved with extraordinary advances in nanofabrication technology. The quantum dot structures are still large, electrodes and contact pads cover extensive space, and they operate only at very low temperatures. Furthermore, the electron beam lithography cannot be used to manufacture large numbers of complex circuits. Thus, since a single quantum dot is not particularly useful, new lithographic techniques which allow three dimensional atomic scale control as happens in the self-assembled quantum

dots should be necessarily improved. Besides making millions of quantum dots by specifying the size and the shape of each dot precisely, their potential applications as electronic or optical materials are the second most challenging problem that researchers try to overcome.

1.2 Similarities Between The Quantum Dots and The Real Atoms

The quantum dots have some similarity with the real atoms in the sense that they have an integral number of electrons and there is an energy cost to both remove an electron and add an electron, as with real atoms. Furthermore, the number of electrons confined within the dot may be changed by changing the Fermi energy. This is similar to a change of valence of real atoms which may be done by changing the local chemical potential. The similarity with real atoms is closer for semiconductor dots than for metallic dots since the latter will typically include millions of conduction electrons whilst the former will usually have a small number of electrons.

By measuring energy that is required to add an electron to the quantum dot (electron affinity) or to remove an electron from the dot (ionization energy), one can learn many properties of the quantum dot structures. This can be done by measuring the current through the quantum dot. Fig. 1.6 shows the conductance through a dot as a function of the gate voltage V_g between the gate and the dot, by applying a very small voltage between the source and the drain. The conductance displays sharp resonances that are almost periodic in V_g and the period is the voltage necessary to add one electron to the quantum dot. There

is a simple semiclassical model, named the charging model, which provides a simple explanation of the main properties of the quantum dots and their similarity with real atoms. This model explains the periodic resonances appearing in the conductance measurements [36] in Fig. 1.6.

1.3 The Charging Model

The charging model is quantitatively correct for the metallic quantum dots and qualitatively correct for the semiconductor dots [37]. To understand the model, consider a metallic particle with typical dimensions of a few thousand angstroms or less which is separated from the leads (source and drain) by thin insulators, as shown in Fig. 1.7. The whole structure sits on a large well-insulated metal electrode, called the gate. The energy required to add a charge Q to the neutral metallic particle is $Q^2/2C$ where C is the total capacitance between the metallic particle and the rest of the system. Since charge Q is not a continuous variable, that is, it is quantized, the flow of current requires a Coulomb energy $e^2/2C$ which is needed to add one electron to the metallic particle. Thus, the charge quantization leads to an energy gap that is called the Coulomb blockade preventing the tunneling process. For an electron to tunnel onto the metallic particle, its energy must exceed the Fermi energy of the source lead by $e^2/2C$, and for a hole to tunnel, its energy must be below the Fermi energy by the same amount, $e^2/2C$. Therefore, the energy gap resulting from the Coulombic interaction between the electrons has a total width of e^2/C. If the temperature is low enough, $kT < e^2/2C$, neither the electrons nor the holes can flow from one

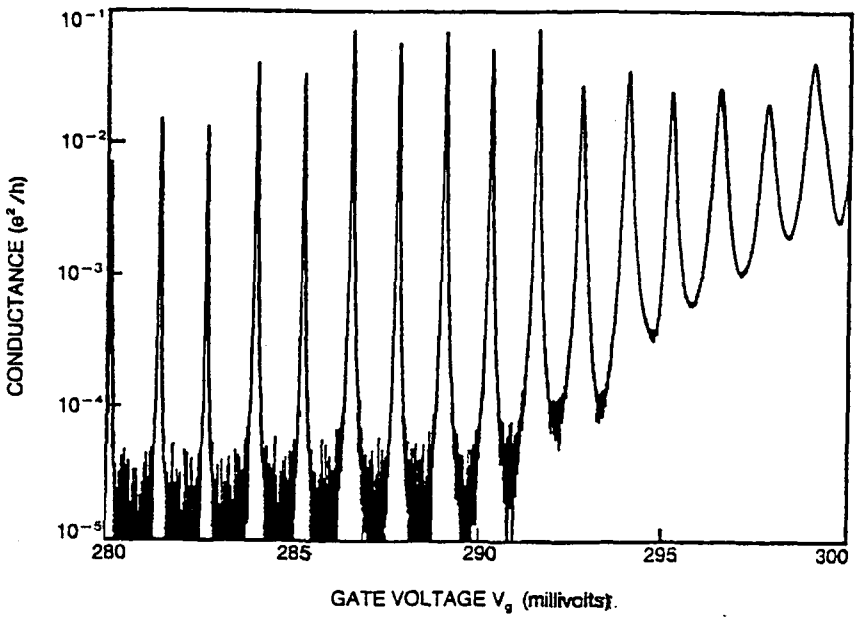

Figure 1.6: Conductance of a semiconductor dot as a function of the gate voltage V_g at a temperature of 60 mK (adapted from Ref. 44).

lead to the other.

By changing the gate voltage V_g that is applied between the gate and the source, the energy required to add charge to the metallic particle can be altered. If the drain-source voltage is very small, which means the source, metallic particle and drain will be at almost the same potential, then the electrostatic energy of a charge Q on the metallic particle is given by

$$E = QV_g + Q^2/2C, \tag{1.1}$$

where the first term is the attractive interaction between Q and the positively charged gate electrode, and the second term is the repulsive interaction (Coulombic interaction) between the bits of charge on the metallic particle. Without the second term, as V_g is increased, the electrons will flow from the leads onto the metallic particle. On the other hand, the large Coulomb repulsion between the

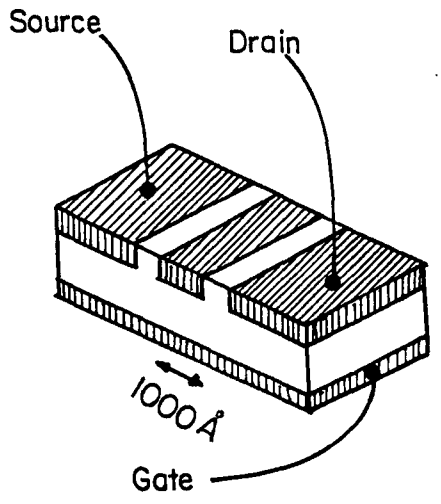

Figure 1.7: Schematic illustration of a metallic quantum dot which is weakly coupled by tunnel barriers to two leads.

charges on the particle opposes this flow of electrons. According to this equation, energy as a function of Q is a parabola with its minimum at $Q_\circ = -CV_g$. However, the number of electrons on the particle is an integer, $Q = -Ne$, so that the charge on the particle can only change by discrete amounts e. In contrast, the electrostatic potential difference of metallic particle and leads changes continuously as the gate voltage, V_g, is altered. This leads to a net charge imbalance $CV_g - Ne$ between the particle and the leads, oscillating in a saw-tooth pattern with gate voltage V_g. Tunneling is blocked at low temperatures, except near the degeneracy points of the saw-tooth, where the charge imbalance jumps from $e/2$ to $-e/2$. At these degeneracy points, where the value of charge is $Q_\circ = -e(N + 1/2)$, the energy gap or the Coulomb blockade of tunneling disappears, and the current can flow. The peaks in the conductance are, therefore, periodic, spaced in gate voltage V_g by e/C.

In Fig. 1.8 (a), charge imbalance $Q+CV_g$ arising between the particle and the

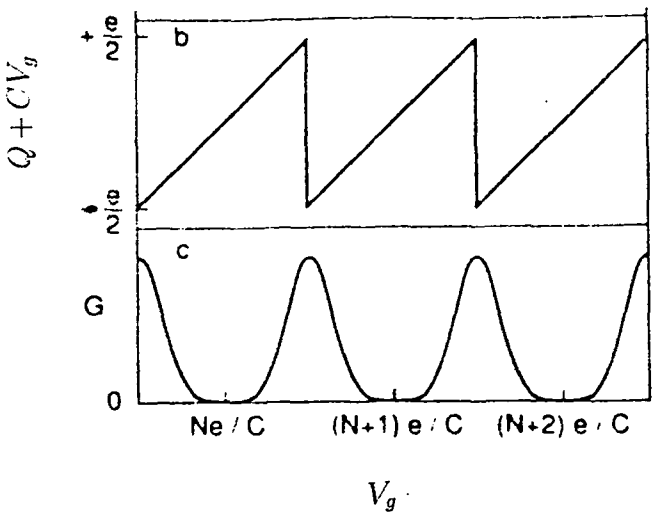

Figure 1.8: a) Charge imbalance $Q + CV_g$ arising between the metallic dot and the leads, and b) conductance G as a function of the gate voltage V_g.

leads as a function of gate voltage V_g and in (b) conductance G of the particle as a function of V_g are presented. As is seen clearly, the tunneling is only possible near the charge degeneracy points at which the Coulomb blockade disappears and the conductance exhibits oscillations. At each Coulomb blockade oscillation the charge on the particle increases by one unit. A charge degeneracy point and a conductance peak are obtained every time the gate voltage V_g is increased by e/C which is the amount of voltage to add one electron to the particle.

In the nano-scale metallic particle which has a high density of electrons, the energy spacing between the discrete levels is so small that it can be ignored and the energy spectrum can be considered as effectively continuous. However, in semiconductor quantum dots there are only a few electrons (about 30-60) and sometimes only one or two electrons. Thus, the energy spectrum for the semiconductor quantum dot is discrete, as it is for natural atoms.

One can learn about the energy level spectrum of the quantum dot or the

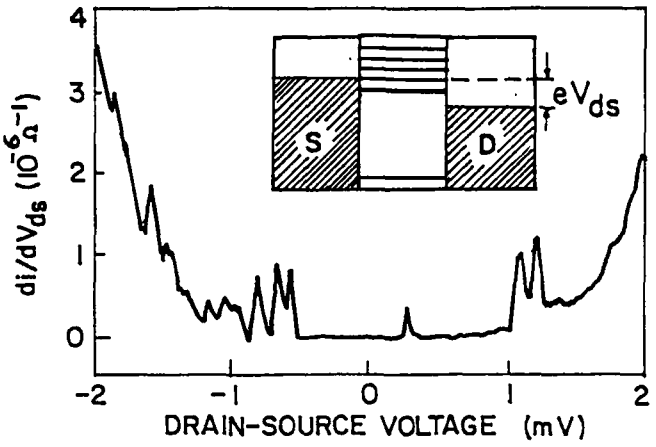

Figure 1.9: Probing the excited states of a semiconductor dot by increasing the voltage V_{ds} (adapted from Ref. 44).

artificial atom by measuring the tunneling current as a function of the voltage V_{ds} between the drain and the source at a fixed value of V_g. When the voltage V_{ds} begins to increase, the Fermi level in the source lead rises relative to the Fermi level in the drain and it also rises relative to the energy levels of the quantum dot. As is seen in Fig. 1.9, the current flows when the Fermi energy of the source is increased above the first quantized energy level of the dot. If the Fermi energy is increased further, the higher excited states of the electrons fall below it, and more current flows through the dot since there exists additional energy levels for tunneling onto the quantum dot. Energy levels can be obtained by measuring the voltage at which there is a peak in the derivative of the current, dI/dV_{ds}.

Increasing the gate voltage, while keeping V_{ds} small, lowers all the energy levels in the artificial atom which has N electrons by eV_g, as shown in Fig. 1.10. The Coulomb blockade gap in the tunneling spectrum also lowers and then completely disappears when the Fermi level in the source and drain becomes degenerate with the $(N+1)$th level of the atom. This gives rise to a peak in the conductance

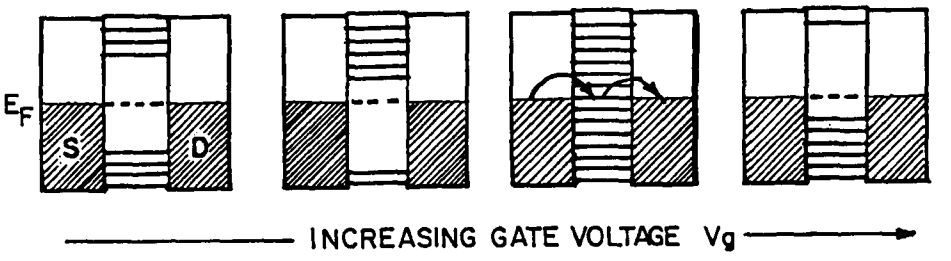

Figure 1.10: Probing the ground state of a semiconductor dot by increasing the voltage V_g.

and an artificial atom which has $N+1$ electrons in its ground state. When V_g is increased further till the Fermi level is degenerate with the $(N+2)$th level, the next conductance peak is reached which means that there exists $N+2$ electrons in the ground state of the artificial atom. Hence, to get from one peak to the next the Fermi energy should be raised by $e^2/C+(E_{N+1}-E_N)$, where E_N is the energy of the Nth level of the atom. If the discrete energy levels are closely spaced, as happens in metallic particles, the Coulomb blockade result is recovered. However, since the level spacing contributes to the energy between successive peaks in the conductance, it should be taken into account together with the charging energy in semiconductor quantum dots.

Thus, the discrete energy levels of the quantum dot or the artificial atom can be probed by altering the drain-source voltage V_{ds}. When the voltage V_{ds} is small compared to the charging energy e^2/C and the level spacing $(E_{N+1}-E_N)$, one can only study the ground state energies of the artificial atom by changing the gate voltage V_g. By increasing the V_{ds} with a considerable amount and keeping the V_g fixed, the excited states of the quantum dot start to contribute to the electron transport.

In conclusion, since the energy spectrum can be treated as continuous in metallic quantum dots and the Coulomb interaction between the electrons is independent of the number of electrons added (known as constant interaction model), the charging model works well. The peaks observed in the conductance are perfectly periodic in the gate voltage. On the other hand in semiconductor quantum dots, the addition energy is given by $e^2/C+\Delta E$ where ΔE is the energy level spacing and it cannot be ignored. Due to extra energy ΔE, which is needed to add a single electron to the dot, the conductance peaks are not perfectly periodic in the gate voltage. Moreover, when adding an electron to the semiconductor quantum dot, some quantum mechanical effects such as the Hund's rule and the Pauli exclusion principle arising from the interactions of the electrons should be also considered. The interactions between the electrons confined in the quantum dot affect its energy spectrum strongly. Various theoretical methods can be used to determine the energy levels of a finite number of electrons in the quantum dot. The Hartree–Fock approximation, the exact diagonalization method and the perturbation theory are the most widely used techniques to investigate the energy spectrum and the effects of the electron–electron interactions. These theoretical methods and the importance of the interaction effects on the electronic properties of a two dimensional quantum dot will be discussed briefly in the subsequent chapters.

CHAPTER 2

TWO–DIMENSIONAL QUANTUM DOTS: FORMULATION

2.1 Fundamental Differences Between The Quantum Dots and The Real Atoms

The fabrication of a quantum dot structure or an artificial atom with controllable number of electrons and geometric structure could be possible, as was mentioned in the Introduction, with the modern semiconductor technology. The dimensions of a quantum dot [38] and the number of electrons confined in it [39-42] could be altered simply by means of the gate voltage. The motion of the electrons in a quantum dot is quantized in all three spatial directions, all having dimensions comparable to the de Broglie wavelength of the particle. However, if the quantization in the vertical direction is much stronger than the quantization in the in-plane directions, a quantum dot could be treated as a disc-like 2D system where the electrons have significant freedom along x- and y- directions.

To have a better insight into the physical properties of the quantum dots it is convenient to compare the light atoms and the few-electron dot structures [43]. As we have summarized in the Introduction, the charging model seems to provide a simple description of the main features of the quantum dots and their similarity to the natural atoms. However, the analogy between the quantum dots and the natural atoms, suggested by the charging model, has certain limitations

due to different energy and length scales of the two systems. In fact, there is now significant evidence, both theoretical and experimental, to support the view that there are some fundamental differences between the natural and the artificial atoms. Using the parabolic band approximation, the energy and the length scales are given by the Rydberg energy and the effective Bohr radius

$$R_y^\star = \frac{m^\star}{m_0 \epsilon^2} R_y, \quad a^\star = \frac{m_0 \epsilon}{m^\star} a, \tag{2.1}$$

respectively, where $m^\star$ (m_0) is the effective (bare) electron mass, and ϵ is the dielectric constant of the medium. These would be, for example, the ground state binding energy ($R_y^\star$) and the corresponding effective Bohr radius ($a^\star$) of a conduction electron bound to a shallow donor ion in a semiconductor. These two quantities can be used to have a quantitative description of the system under concern. Indeed, $R_y^\star(\text{meV}) = 1.36 \times 10^4$, 18, 8, 0.85 and $a^\star(\text{Å}) = 0.529$, 33.4, 82.4, 567 for H, Si, GaAs, InSb, respectively. It is clear that energies of the semiconductors are roughly three orders of magnitude below that of the Hydrogen atom whereas their radii are roughly two orders of magnitude above. This hierarchy of the effective Bohr radius and Rydberg guarantees that, for natural atoms, the mean kinetic energy remains greater than the mean Coulomb repulsion among the electrons. For instance, in He the mean kinetic energy is twice greater than the Coulomb repulsion energy between the two 1s electrons. For this reason, the free electron approximation works very well for natural atoms. In fact, the Hartree–Fock (HF) approximation, which ignores the correlation effects among the electrons, is sufficient to have a quantitative description of the light atoms.

However, as the effective Bohr radii and the Rydbergs of the sample semiconductors show, generally mean kinetic energy for such systems is well below the Coulomb repulsion energy between the electrons. Therefore, it is almost unlikely to expect the HF approximation to work for large quantum dots.

To have a clear understanding of the dominance of the Coulombic repulsion energy over the mean kinetic energy, we assume two electrons in a quantum box with sides of length L and infinite potential barriers. The level splitting between one electron energy levels goes like $\delta E \sim \hbar^2/(m^* L^2)$. On the other hand, the Coulomb repulsion energy is $V \sim e^2/(\epsilon\epsilon_0 L)$. Therefore, $\delta E/V \sim a^*/L$ which shows that for sufficiently large dots and fixed electron number the Coulombic repulsion energy between the electrons dominates on the mean kinetic energy.

Although quantum dots and natural atoms contain comparable number of electrons, their electronic properties can have huge differences due to the nature of the confinement potential [43]. In quantum dots the confinement potential is experimentally controllable [44]; and usually the lateral confinement potential is created by electrostatically squeezing the planar charge distribution in the 2DEG. Therefore, it shows a parabolic characteristic ($\sim r^2$) which is much shallower than the $1/r$ potential of the natural atoms, and seems to represent fairly well the electrostatically confined electrons. The advantage of using a harmonic type of confinement potential is the analytical simplicity of the problem, since the center of mass and the relative coordinates decouple. However, in the far-infrared spectroscopy, the radiation field cannot detect the electron-electron correlations when the confinement potential is parabolic. This is caused by decoupling of the

far-infrared radiation with the relative motion of electrons [45].

Thus, in order to probe the interaction effects among the electrons, it has been suggested that the shape of the dot should be modified to achieve the coupling of the center of mass and the relative motions [45]. Besides these, some authors have achieved this coupling with deviations from the exact harmonic confinement [46-48]. Rather than electrostatically confined quantum dots which are usually described with a harmonic potential, quantum dots can also be manufactured by etching techniques or self organized growth which have a hard-wall type confinement potential [49]. Since the center of mass motion of the electrons is coupled with their relative part in this type of confinement potential, the effects of correlation influencing energy spectrum, transport, and spectral measurements can be studied with the excitation spectra [50].

2.2 Hamiltonian in The Second Quantization Language

In this work we consider a few electron system in a two dimensional circular quantum dot of radius a. The longitudinal and the transverse coordinates are denoted as z and $\vec{\mathbf{r}} = (\rho, \theta)$ respectively, so that the three– dimensional coordinate is $\vec{\mathbf{x}} = (z, \vec{\mathbf{r}})$. The width of the quantum dot is assumed to be much smaller than its radius, $w << a$, in all of the analytical and numerical analysis.

An N- electron system is described by the Hamiltonian

$$H = \sum_{i=1}^{N} \{ -\frac{\hbar^2}{2m^*} \vec{\nabla}_i^2 + U(\vec{\mathbf{x}}_i) \} + \frac{e^2}{2\epsilon} \sum_{i \neq j} \frac{1}{|\vec{\mathbf{x}}_i - \vec{\mathbf{x}}_j|} , \tag{2.2}$$

where m^* is the electron effective mass and ϵ is the dielectric constant of the

medium. The second term in the parenthesis, $U(\vec{\mathbf{x}})$, is the hard-wall type confinement potential which vanishes for $|\vec{\mathbf{x}}| < a$, and infinite for $|\vec{\mathbf{x}}| \geq a$. By using a as the unit of length, that is rescaling $|\vec{\mathbf{x}}|$ in Eq. (2.2), one can obtain

$$H = \frac{\hbar^2}{m^* a^2} \sum_{i=1}^{N} (-\frac{1}{2}) \vec{\nabla}_i^2 + \frac{e^2}{2\epsilon a} \sum_{i \neq j} \frac{1}{|\vec{\mathbf{x}}_i - \vec{\mathbf{x}}_j|} \,. \tag{2.3}$$

The terms within the sums in Eq. (2.3) are now dimensionless. Introducing the dimensionless coupling constant $\lambda = a/a_B$ converts the Eq. (2.3) to

$$H = \frac{\hbar^2}{m^* a_B^2 \lambda^2} \sum_{i=1}^{N} (-\frac{1}{2}) \vec{\nabla}_i^2 + \frac{e^2}{2\epsilon a} \sum_{i \neq j} \frac{1}{|\vec{\mathbf{x}}_i - \vec{\mathbf{x}}_j|} \,. \tag{2.4}$$

By inserting the effective Bohr radius $a_B = \epsilon \hbar^2/(m^* e^2)$ into the equation above, we obtain the dimensionless Hamiltonian $\mathcal{H}$ via the definition

$$H = \frac{\hbar^2}{m^* a_B^2 \lambda^2} \mathcal{H}, \tag{2.5}$$

where

$$\mathcal{H} = \sum_{i=1}^{N} (-\frac{1}{2}) \vec{\nabla}_i^2 + \frac{\lambda}{2} \sum_{i \neq j} \frac{1}{|\vec{\mathbf{x}}_i - \vec{\mathbf{x}}_j|}. \tag{2.6}$$

One recalls that the energy is measured in units of $\hbar^2/(m^* a_B^2 \lambda^2)$ which depends on λ, and the length is measured in units of a, the dot radius.

To express the dimensionless Hamiltonian $\mathcal{H}$ in the second quantization language, one inserts the density operator $\varrho(\vec{\mathbf{x}}) = \Psi^\dagger(\vec{\mathbf{x}})\Psi(\vec{\mathbf{x}})$ into the Eq. (2.6)

$$\mathcal{H} = \mathcal{A} \sum_{i=1}^{N} \Psi^\dagger(\vec{\mathbf{x}}_i)(-\frac{1}{2}) \vec{\nabla}_i^2 \Psi(\vec{\mathbf{x}}_i) + \mathcal{A}^2 \frac{\lambda}{2} \sum_{i \neq j} V(\vec{\mathbf{x}}_i - \vec{\mathbf{x}}_j) \Psi^\dagger(\vec{\mathbf{x}}_i)$$
$$\Psi^\dagger(\vec{\mathbf{x}}_j)\Psi(\vec{\mathbf{x}}_j)\Psi(\vec{\mathbf{x}}_i) \,, \tag{2.7}$$

where $\mathcal{A}$ is the area and $\Psi(\vec{\mathbf{x}}) = \sum_K a_K \varphi_K(\vec{\mathbf{x}})$ is the many particle eigenstate with annihilation operator a_K and single particle eigenstate $\varphi_K(\vec{\mathbf{x}})$. By transforming

the summations over i and j into the integrals, using the well– known identity: $\sum_i \longrightarrow \frac{1}{\mathcal{A}} \int d^2x$, the dimensionless Hamiltonian becomes

$$\mathcal{H} = \sum_{K,L} a_K^\dagger a_L \int d^2x \varphi_K^\dagger(\vec{\mathbf{x}})(-\frac{1}{2})\vec{\nabla}^2 \varphi_L(\vec{\mathbf{x}}) + \frac{\lambda}{2} \sum_{K,L,M,N} a_K^\dagger a_L^\dagger a_M a_N$$
$$\int\int d^2x d^2x' V(\vec{\mathbf{x}} - \vec{\mathbf{x}}') \varphi_K^\dagger(\vec{\mathbf{x}}) \varphi_L^\dagger(\vec{\mathbf{x}}') \varphi_M(\vec{\mathbf{x}}') \varphi_N(\vec{\mathbf{x}}). \tag{2.8}$$

Introducing the single particle energy level $\mathcal{E}_K$ and the Coulomb matrix element $V_{K,L,M,N}$, the Hamiltonian takes the form

$$\mathcal{H} = \sum_K \mathcal{E}_K a_K^\dagger a_K + \frac{\lambda}{2} \sum_{K,L,M,N} V_{K,L,M,N}\, a_K^\dagger a_L^\dagger a_M a_N \ , \tag{2.9}$$

where

$$\mathcal{E}_K = \int d^2x \varphi_K^\dagger(\vec{\mathbf{x}})(-\frac{1}{2})\vec{\nabla}^2 \varphi_K(\vec{\mathbf{x}}) \ , \tag{2.10}$$

and

$$V_{K,L,M,N} = \int\int d^2\vec{\mathbf{x}} d^2\vec{\mathbf{x}}' V(\vec{\mathbf{x}} - \vec{\mathbf{x}}') \varphi_K^\dagger(\vec{\mathbf{x}}) \varphi_L^\dagger(\vec{\mathbf{x}}') \varphi_M(\vec{\mathbf{x}}') \varphi_N(\vec{\mathbf{x}}) \ . \tag{2.11}$$

In these equations $\varphi_A(\vec{\mathbf{x}})$ is the single particle eigenstate of the free Hamiltonian, and $A(= K, L, M, N)$ is a collective index designating the radial (n_A), angular momentum (m_A) and spin (σ_A) quantum numbers. The solution of the eigenvalue problem for the free Hamiltonian yields

$$\varphi_A(\vec{\mathbf{x}}) = \phi_{n_A,m_A}(\vec{\mathbf{x}}) \chi_{\sigma_A} \ , \tag{2.12}$$

where χ_σ is the spin wavefunction, and $\phi_{n,m}(\vec{\mathbf{x}})$ is the normalized orbital eigenfunction

$$\phi_{n,m}(\vec{\mathbf{x}}) = \frac{1}{\sqrt{\pi}} \frac{1}{|J_{|m|+1}(k_{n,|m|})|} e^{im\theta} J_{|m|}(k_{n,|m|}|\vec{\mathbf{x}}|) \ . \tag{2.13}$$

Using Eqs. (2.12) and (2.13) in (2.10) one gets the eigenvalues $\mathcal{E}_K = \frac{1}{2}k^2_{n_K,|m_K|}$ which are independent of the spin and the sign of m. Here $k_{n,|m|}$ are the zeroes of the Bessel function ($J_{|m|}(k_{n,|m|}) = 0$).

As the normalized orbital eigenfunctions in Eq. (2.13) depend already on the Bessel functions, it is practically convenient to expand the Coulomb potential, $V(\vec{\mathbf{x}} - \vec{\mathbf{x}}') = 1/|\vec{\mathbf{x}} - \vec{\mathbf{x}}'|$, in terms of the Bessel functions as well

$$\frac{1}{|\vec{\mathbf{x}} - \vec{\mathbf{x}}'|} = \sum_{m=-\infty}^{\infty} \int_0^{\infty} dk\; e^{im(\theta-\theta')} J_{|m|}(k\rho) J_{|m|}(k\rho') e^{-k(z_> - z_<)}, \tag{2.14}$$

where $z_> - z_<$ shows the extension of the dot in the longitudinal direction. If the longitudinal extension of the dot is a non-negligible fraction of its in-plane size, one has to analyze the excitations in this direction, too. However, in the limit of $z_> - z_< \to 0$, it is sufficient to probe only the transverse plane assuming that the system is in the lowest state for longitudinal dynamics. In the following, we follow the latter one and give a small value to $z_> - z_<$ in the calculations. In this approximation, by using Eqs. (2.12), (2.13) and (2.14) in (2.11), we obtain the equation (2.15) as the matrix element of the Coulomb potential. Here we note that the angular integrations in $V_{K,L,M,N}$ impose the selection rule $m_K - m_L = m_N - m_M$ otherwise $V_{K,L,M,N}$ vanishes.

$$\begin{aligned} V^{n_K,n_L,n_M,n_N}_{m_K,m_L,m_M,m_N} &= 4 \frac{1}{|J_{|m_K|+1}(k_{n_K,|m_K|})|} \frac{1}{|J_{|m_L|+1}(k_{n_L,|m_L|})|} \\ &\frac{1}{|J_{|m_M|+1}(k_{n_M,|m_M|})|} \frac{1}{|J_{|m_N|+1}(k_{n_N,|m_N|})|} \int_0^{\infty} dk \int_0^1 d\rho\, \rho \\ &J_{|m_K|}(k_{n_K,|m_K|}\rho) J_{|m_L|}(k_{n_L,|m_L|}\rho) J_{|m_K - m_L|}(k\rho) \\ &\int_0^1 d\rho'\, \rho' J_{|m_M|}(k_{n_M,|m_M|}\rho') J_{|m_N|}(k_{n_N,|m_N|}\rho') J_{|m_N - m_M|}(k\rho') \,. \end{aligned} \tag{2.15}$$

Since one can play with the dimensionless coupling constant λ which means that it is a changeable parameter, a quantum dot goes between a bulk sample and a real atom. Therefore, the quantum dot is a perfect structure to study the many particle systems and electron-electron interactions. By increasing the coupling constant λ, the quantum mechanical system of weakly interacting particles turns into a strongly correlated quasiclassical system which forms Wigner molecule for sufficiently large λ value.

Most of the properties in a quantum dot including spectroscopy measurements [42,51-53], tunneling currents and charging energies [15,54-60] depend on the energy spectrum of the electron system. Thus, the main problem that should be analyzed is to obtain the eigensolutions of a system consisting of interacting electrons confined in a quantum dot. Various theoretical methods have been developed to study the energy spectrum of a finite number of electrons in quantum dots of different confinement potentials and geometric structures [38,45,47,49,61-70]. The Hartree–Fock approximation is the most widely used technique when the number of electrons in the quantum dot is large. In the high electron density limit which means that the mean separation between electrons is small, the kinetic energy dominates over the potential energy and, therefore, the Hartree–Fock approximation works well for weakly interacting many particle system. On the other hand at low electron densities, the Coulombic potential energy dominates over the kinetic energy and thus electrons occupy energetically favorable fixed positions within the dot. In this limit the Hartree–Fock approximation cannot give correct results due to the correlations between the electrons.

Another mostly preferred method to get the energy spectrum of a quantum dot is the exact diagonalization of the Hamiltonian in the space of many particle wave functions when the number of electrons is small [50,71]. In addition, the perturbation technique is also frequently used to get an analytical dependence of the energy on the quantum dot size. But unfortunately, since the Coulomb series is usually divergent, it can be applied only for small λ values. To improve the convergence of the perturbation series and to enable its application for large λ values, the renormalized perturbation technique can be used in studies of many particle systems [72,73].

2.3 The Exact Diagonalization Method

For calculating the physical quantities such as energy eigenvalues, charge density and the pair correlation function, one needs to compute the matrix elements of the Hamiltonian operator between the N- electron ground state which can be expressed as

$$|\Phi_0^{(N)}>=\sum_C b_C^0|C>, \tag{2.16}$$

where $|C>= a^\dagger_{n_1,m_1,\sigma_1}....a^\dagger_{n_N,m_N,\sigma_N}|0>$ is a non-interacting Slater determinant and b_C^0 are the expansion coefficients. Here the sum runs over all possible configurations of the quantum numbers including radial, orbital, and spin quantum numbers. The expansion coefficients b_C^0 for each configuration $|C>$ are computed by diagonalizing the Hamiltonian matrix in the N- electron ground state, $|\Phi_0^{(N)}>$.

For the circular quantum dot geometry, in addition to the total spin S, $S_z = \sum_{i=1}^{N} \sigma_i$ and the z- component of the total orbital angular momentum $M = \sum_{i=1}^{N} m_i$ are good quantum numbers. In fact, this is evident from the radial (n), orbital angular momentum (m), and spin (σ) dependencies of the single particle eigenfunctions (2.12,2.13). Due to these symmetry properties we will be interested in those many electron states having fixed values of M and S_z for a given electron number, N. Moreover, we will restrict ourselves to those states for which $S_z = S$. In what follows we will consider a circular quantum dot containing 2, 3 and 4 electrons. Below we list one by one the basis states $|C>$ corresponding to the relevant cases mentioned above.

For 2 electrons, there are two basis functions coming from triplet and singlet states:

$$|S = S_z = 1, N = 2> = a^{\dagger}_{\alpha,\uparrow} a^{\dagger}_{\beta,\uparrow} |0>, \tag{2.17}$$

$$|S = S_z = 0, N = 2> = \frac{1}{\sqrt{2}} \left(a^{\dagger}_{\alpha,\uparrow} a^{\dagger}_{\beta,\downarrow} - a^{\dagger}_{\alpha,\downarrow} a^{\dagger}_{\beta,\uparrow} \right) |0> . \tag{2.18}$$

For three electrons, there are three basis states. While the first one corresponds to the quartet state

$$|S = S_z = 3/2, N = 3> = a^{\dagger}_{\alpha,\uparrow} a^{\dagger}_{\beta,\uparrow} a^{\dagger}_{\gamma,\uparrow} |0>, \tag{2.19}$$

the other two states represent the doublet configurations

$$\begin{aligned} |S = S_z = 1/2, N = 3> &= \frac{1}{\sqrt{6}} \Big(2\, a^{\dagger}_{\alpha,\downarrow} a^{\dagger}_{\beta,\uparrow} a^{\dagger}_{\gamma,\uparrow} - a^{\dagger}_{\alpha,\uparrow} a^{\dagger}_{\beta,\downarrow} a^{\dagger}_{\gamma,\uparrow} \\ &- a^{\dagger}_{\alpha,\uparrow} a^{\dagger}_{\beta,\uparrow} a^{\dagger}_{\gamma,\downarrow} \Big) |0> \end{aligned} \tag{2.20}$$

$$|S = S_z = 1/2, N = 3> = \frac{1}{\sqrt{2}} \left(a^{\dagger}_{\alpha,\uparrow} a^{\dagger}_{\beta,\uparrow} a^{\dagger}_{\gamma,\downarrow} - a^{\dagger}_{\alpha,\uparrow} a^{\dagger}_{\beta,\downarrow} a^{\dagger}_{\gamma,\uparrow} \right) |0> . \tag{2.21}$$

For four electrons there are quintet (S=2), triplet (S=1), and singlet (S=0) configurations. The triplet configurations have three distinct states

$$|S=S_z=1,N=4> = \frac{1}{\sqrt{2}}\left(a^\dagger_{\alpha,\downarrow}a^\dagger_{\beta,\uparrow}a^\dagger_{\gamma,\uparrow}a^\dagger_{\eta,\uparrow} - a^\dagger_{\alpha,\uparrow}a^\dagger_{\beta,\downarrow}a^\dagger_{\gamma,\uparrow}a^\dagger_{\eta,\uparrow}\right)|0>, \quad (2.22)$$

$$\begin{aligned}|S=S_z=1,N=4> &= \frac{1}{\sqrt{6}}\left(a^\dagger_{\alpha,\downarrow}a^\dagger_{\beta,\uparrow}a^\dagger_{\gamma,\uparrow}a^\dagger_{\eta,\uparrow} + a^\dagger_{\alpha,\uparrow}a^\dagger_{\beta,\downarrow}a^\dagger_{\gamma,\uparrow}a^\dagger_{\eta,\uparrow}\right.\\ &- \left. 2\,a^\dagger_{\alpha,\uparrow}a^\dagger_{\beta,\uparrow}a^\dagger_{\gamma,\downarrow}a^\dagger_{\eta,\uparrow}\right)|0>, \end{aligned} \quad (2.23)$$

$$\begin{aligned}|S=S_z=1,N=4> &= \frac{1}{\sqrt{12}}\left(a^\dagger_{\alpha,\downarrow}a^\dagger_{\beta,\uparrow}a^\dagger_{\gamma,\uparrow}a^\dagger_{\eta,\uparrow} + a^\dagger_{\alpha,\uparrow}a^\dagger_{\beta,\downarrow}a^\dagger_{\gamma,\uparrow}a^\dagger_{\eta,\uparrow}\right.\\ &+ \left. a^\dagger_{\alpha,\uparrow}a^\dagger_{\beta,\uparrow}a^\dagger_{\gamma,\downarrow}a^\dagger_{\eta,\uparrow} - 3\,a^\dagger_{\alpha,\uparrow}a^\dagger_{\beta,\uparrow}a^\dagger_{\gamma,\uparrow}a^\dagger_{\eta,\downarrow}\right)|0>, \end{aligned} \quad (2.24)$$

and two singlet bases are given by

$$\begin{aligned}|S=S_z=1,N=4> &= \frac{1}{2}\left(a^\dagger_{\alpha,\downarrow}a^\dagger_{\beta,\downarrow}a^\dagger_{\gamma,\uparrow}a^\dagger_{\eta,\uparrow} - a^\dagger_{\alpha,\downarrow}a^\dagger_{\beta,\uparrow}a^\dagger_{\gamma,\downarrow}a^\dagger_{\eta,\uparrow}\right.\\ &- \left. a^\dagger_{\alpha,\uparrow}a^\dagger_{\beta,\downarrow}a^\dagger_{\gamma,\uparrow}a^\dagger_{\eta,\downarrow} + a^\dagger_{\alpha,\uparrow}a^\dagger_{\beta,\uparrow}a^\dagger_{\gamma,\downarrow}a^\dagger_{\eta,\downarrow}\right)|0>, \end{aligned} \quad (2.25)$$

$$\begin{aligned}|S=S_z=1,N=4> &= \frac{1}{\sqrt{12}}\left(a^\dagger_{\alpha,\downarrow}a^\dagger_{\beta,\downarrow}a^\dagger_{\gamma,\uparrow}a^\dagger_{\eta,\uparrow} + a^\dagger_{\alpha,\downarrow}a^\dagger_{\beta,\uparrow}a^\dagger_{\gamma,\downarrow}a^\dagger_{\eta,\uparrow}\right.\\ &- 2\,a^\dagger_{\alpha,\downarrow}a^\dagger_{\beta,\uparrow}a^\dagger_{\gamma,\uparrow}a^\dagger_{\eta,\downarrow} - 2\,a^\dagger_{\alpha,\uparrow}a^\dagger_{\beta,\downarrow}a^\dagger_{\gamma,\downarrow}a^\dagger_{\eta,\uparrow}\\ &+ \left. a^\dagger_{\alpha,\uparrow}a^\dagger_{\beta,\downarrow}a^\dagger_{\gamma,\uparrow}a^\dagger_{\eta,\downarrow} + a^\dagger_{\alpha,\uparrow}a^\dagger_{\beta,\uparrow}a^\dagger_{\gamma,\downarrow}a^\dagger_{\eta,\downarrow}\right)|0>, \end{aligned} \quad (2.26)$$

where each of the indices α, β, γ and η stands for the pair of radial and orbital angular momentum quantum numbers. With these basis states at hand, one can construct the Hamiltonian matrix by evaluating the matrix elements of (2.9). Under the constraints following from the fixed M and S_z values, a Hamiltonian matrix is formed in space of $\alpha, \beta, \ldots$. Due to the large amount of computer memory needed for the evaluation of the Hamiltonian matrix elements, the eigensolution of the Hamiltonian could be obtained only for very small N. For the same reason it is necessary to cut off n and m at a large enough value for not to spoil the precision

of the computation. It is clear that this procedure truncates the semi-infinite Hamiltonian matrix to a finite one. Diagonalization of the latter yields the energy eigenvalues and the eigenvectors, b_C^0 of the few electron system. After obtaining the expansion coefficients b_C^0 in this way, one turns to the computation of other physical quantities such as charge density and the pair correlation function.

If one is interested in the transport properties of the dot [50], then it is necessary to study the energy spectrum for each basis state listed above. Though the main concern of this work is not on the transport properties, the energy spectrum of each basis state for 2, 3 and 4 electrons is analyzed and the results are presented in Chapter 3.

2.4 Charge Density and The Pair Correlation Function in The Second Quantization Language

Other than the energy spectrum, charge density and the pair correlation function are important by themselves as they provide information about the electron distribution in the quantum dot. Studies of the quantum dots with parabolic confinement potentials [74] show that the three-electron wave function is peaked at the vertices of an equilateral triangle. The side length of this triangle is determined by the distance r_0 which minimizes the total potential energy of the system. This triangular structure is the best for binding; however, there are certain selection rules following from S_z and M. The necessary c[illegible]n for doublet states, $S_z = 1/2$, to have an equilateral triangular struct[illegible] $(k = 0, 1, 2, ...)$. Similarly for $S_z = 3/2$ only for $M = 3k$ an equi[illegible]

structure is formed. When $S_z = 3/2$ ($S_z = 1/2$), $M = 0$ ($M = 1$) minimizes the energy with an equilateral triangular structure. Once such a structure is formed with these smallest possible k values, it remains to be the ground state for higher values of k, such that the larger the k, the higher the energy.

When the type of confinement potential is changed to a hard-wall one, however, such a characteristic length r_0 cannot be obtained analytically at all. However, guided by the studies of 1D hard-wall potentials in [75], one still expects a triangular structure to arise, especially for large enough dots. In Chapter 3, we will discuss in detail the charge density and the pair correlation function for $S_z = 3/2$ case for different dot sizes. Therefore, below we give the formulae for the charge density and the pair correlation function for the quartet state (2.19) only.

In general, the charge density of N electrons is given by

$$\rho(\vec{x}) = \sum_{\sigma} < \Phi_0^{(N)} | \Psi_\sigma^\dagger(\vec{x}) \Psi_\sigma(\vec{x}) | \Phi_0^{(N)} >, \tag{2.27}$$

which measures the electron density at a given point $\vec{x}$ in space. Representing $\{n_1, m_1, \uparrow\}$ by β_1, $\{n_2, m_2, \uparrow\}$ by β_2, and $\{n_3, m_3, \uparrow\}$ by β_3, and inserting the field operator $\Psi_\sigma(\vec{x})$, equations (2.16) and (2.19) into (2.27), we get

$$\rho(\vec{x}) = \sum_{C,C'} b_C^0 b_{C'}^0 \sum_{K,L} < 0 | a_{\beta_3'} a_{\beta_2'} a_{\beta_1'} \{\phi_K^\dagger(\vec{x}) a_K^\dagger\} \{\phi_L(\vec{x}) a_L\}$$
$$a_{\beta_1}^\dagger a_{\beta_2}^\dagger a_{\beta_3}^\dagger | 0 > . \tag{2.28}$$

One can obtain the final form of the charge density for three electrons confined in a circular quantum dot by acting the operator a_L to the right and the $a_K^\dagger$ to the left via the anti-commutator relation $\{a_L, a_{\beta_1}^\dagger\} = \delta_{L,\beta_1}$.

Another relevant quantity, the pair correlation function, is a two-point function defined by

$$\rho_c(\vec{x},\vec{x}') = \sum_{\sigma,\sigma'} < \Phi_0^{(N)}|\Psi_\sigma^\dagger(\vec{x})\Psi_{\sigma'}^\dagger(\vec{x}')\Psi_{\sigma'}(\vec{x}')\Psi_\sigma(\vec{x})|\Phi_0^{(N)} >, \tag{2.29}$$

which is the probability of finding an electron at $\vec{x}$ given that another one is situated at $\vec{x}'$. Similar to the charge density, one can easily write down the pair correlation function in terms of the creation and the annihilation operators

$$\rho_c(\vec{x},\vec{x}') = \sum_{C,C'} b_C^0 b_{C'}^0 \sum_{K,L} < 0|a_{\beta_3'}a_{\beta_2'}a_{\beta_1'}\{\phi_K^\dagger(\vec{x})a_K^\dagger\}\{\phi_L^\dagger(\vec{x}')a_L^\dagger\}$$
$$\{\phi_L(\vec{x}')a_L\}\{\phi_K(\vec{x})a_K\}a_{\beta_1}^\dagger a_{\beta_2}^\dagger a_{\beta_3}^\dagger|0> . \tag{2.30}$$

In this equation two annihilation operators a_L and a_K are acting to the right and two creation operators $a_K^\dagger$ and $a_L^\dagger$ are acting to the left again via the anti-commutator relation $\{a_K, a_{\beta_1}^\dagger\} = \delta_{K,\beta_1}$.

CHAPTER 3

NUMERICAL ANALYSIS

3.1 Three– and Two–Dimensional Electron Gases: The Wigner Crystallization

It is well known that the behavior of Coulombically interacting electrons in a nonresponsive, uniform, positive neutralizing background charge is quite different in the high and low electron density limits. The system is characterized by the dimensionless density parameter $r_s = a/a_\circ$ which is the Wigner-sphere radius in units of Bohr radii. At high electron densities (small r_s) comparable with that in real metals, the kinetic energy dominates the potential energy (Coulomb repulsion) and the system at low energies can be treated by independent electron model [76] in which the electrons are fully delocalized. However, at low density limit (large r_s), delocalized picture of electrons completely breaks down and once the Coulombic potential energy dominates over the kinetic energy, the electrons avoid each other maximally [77]. In this situation, electrons localize on the sites of a lattice and one can find the stable lattice by minimizing the Madelung energy. So far, studies on this subject have proved that the *bcc* lattice has the lowest Madelung energy.

The transition from a weakly coupled electron liquid to a Wigner crystal at

a large enough r_s value is revealed as a result of the effects of correlation. Electron correlations play an important role in determining the physical properties of a many-body system and can be treated quantitatively in various models at all electron densities. The Hartree-Fock solution for the jellium model yields a ground state energy in units of Rydberg as $r_s \to 0$

$$E_{HF}/N = (\frac{2.21}{r_s^2} - \frac{0.916}{r_s})\ Ry\ . \tag{3.1}$$

Many-body perturbation on this state in which electrons are completely delocalized gives an approximate value of the correlation energy E_c, defined as the difference between the true ground state energy E_o and its Hartree-Fock approximation E_{HF} [78]. As $r_s \to \infty$, Wigner has shown that the system can further lower its energy after the crystallization of the system in a Wigner solid. In this limit, the energy per particle in the Wigner solid is asymptotically given by

$$E/N = (\frac{-1.79}{r_s} + \frac{2.66}{r_s^{3/2}})\ Ry \tag{3.2}$$

which has a quite different behavior than the Hartree–Fock energy given above.

At zero temperature, two methods have been mainly used to calculate the correlation energies for many electron systems: configuration interaction and many-body perturbation theory [79,80]. However, important progress in the calculation of the correlation energy has been achieved by using the quantum Monte Carlo (QMC) method which provides the electronic correlation energy very accurately. In this approach, the aim is to obtain the exact ground state wave function of a many-body system by solving the Schrodinger equation numerically. The QMC method was successfully applied to the jellium model in Ref. [81]. The authors

have calculated the correlation energies for both charged bosons and fermions by an exact stochastic simulation of the Schrodinger equation at zero temperature. In this simulation, it is found that the ferromagnetic or polarized Fermi fluid undergoes Wigner crystallization at $r_s = 100 \pm 20$. Later, again by using Monte Carlo simulations, the ground state properties of the two-dimensional electron gas have been analyzed in the liquid and solid phases (in the density range $1 \leq r_s \leq 100$) [82]. At small r_s, the electrons form a weakly coupled Fermi liquid whereas at large r_s they undergo a Wigner crystallization similar to the three-dimensional electron gas. However, in the 2D electron systems, electrons are localized on a two-dimensional hexagonal lattice which has already the lowest Madelung energy, and the Wigner crystallization is observed at the density $r_s \simeq 37 \pm 5$. The observation of the Wigner crystallization is also an extremely challenging problem from the experimental point of view. Although obtaining a low-defect region with sufficiently low electron density is experimentally difficult, evidence of Wigner crystallization has been reported in a two-dimensional electron system formed at the semiconductor heterojunctions [83,84].

3.2 Few Electrons in a One–Dimensional Quantum Dot

The analogue of Wigner crystallization for large quantum dots with just a few electrons is also an interesting and attractive subject. Compared to an infinite system in which only the density-density correlation function crystallizes, the charge density distribution may also crystallize with the electrons occupying energetically favored positions within the dot. By the resemblance to the

Wigner lattice, large quantum dots with large mean separation between electrons have been called Wigner molecules [75,85]. Another attractive aspect of studying the few-electron quantum dot systems follows from the possibility of performing an exact analysis by the numerical diagonalization of the Hamiltonian matrix [38,61,86]. However, this method is expensive on computer time to solve more than a few electrons such that the practical limit is $N = 5$ in one dimensional quantum dots and $N = 3$ in two dimensional dot systems. For high density quantum dots, one can obtain reasonable results with the independent electron model using the Hartree-Fock approximation which is actually valid for infinite systems. The numerical calculations treating the ground state of the interacting electrons ($10 \leq N \leq 30$) in a circular dot with parabolic confinement potential in the Hartree approximation have reproduced the exact results very well [47]. In addition, the random phase approximation (RPA) calculations in the same work have provided a good qualitative understanding of some far infrared radiation (FIR) experiments [56].

The independent electron model is a poor approximation when the mean electron separation in the dot is large, and it gives qualitatively incorrect results. This has been proved by the exact diagonalization for a one-dimensional quantum dot with a rectangular well confining potential [75,87]. Fig. 3.1 taken from [87] shows the energy spectrum for $N = 1$ to $N = 4$ for a well width $L = 9.45a_B$. As is seen in this figure, the energy spectrum consists of a series of multiplets and the energy separation between multiplets is much greater than the energy splitting within a multiplet. Furthermore, by investigating the lowest multiplet

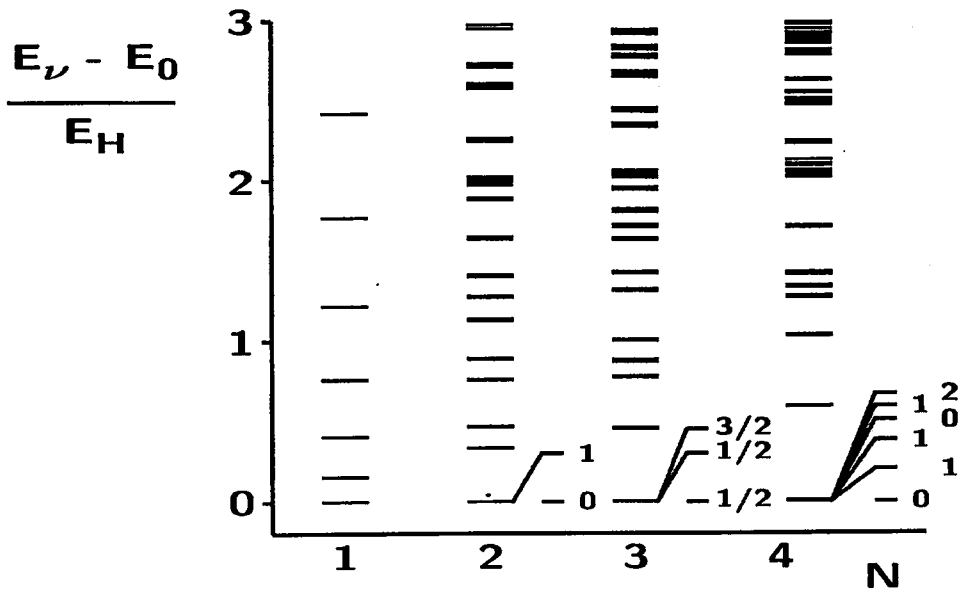

Figure 3.1: Energy spectra for various N and $L = 9.45a_B$ in a one–dimensional quantum dot. For clarity, the lowest multiplets are magnified indicating the total spin of each level

with $N = 3$ electrons, one can easily see the incapability of the independent electron picture which would give a doublet lowest followed by further doublets at energies $\mathcal{E}_1 - \mathcal{E}_0$ and $\mathcal{E}_2 - \mathcal{E}_1$ relative to the ground state, and an octet at energy $\mathcal{E}_2 - \mathcal{E}_0$ etc., where $\mathcal{E}_n$ is the single electron level. However, the exact diagonalization results give the lowest multiplet consisting of doublet, doublet, quartet with very small splitting between them ($\ll \mathcal{E}_1 - \mathcal{E}_0$), followed by a relatively large gap to another multiplet with closely spaced energy levels. The energy spectrum given in Fig. 3.1 can be understood clearly by plotting the charge density of all three electrons in the ground state of the interacting system for different values of L. In this charge density plot, Fig. 3.2 taken from [75], when $L = 0.1a_B$, the Coulomb interaction perturbs the kinetic energy only weakly, such that the total charge density is dominated by the lowest occupied one-electron energy levels.

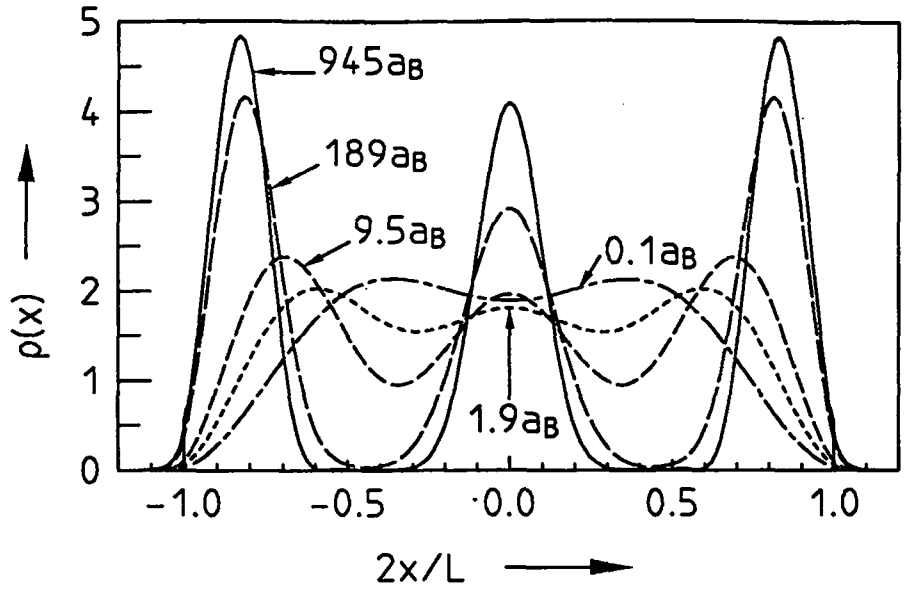

Figure 3.2: Charge density for $N = 3$ and for different L ($0.1a_B \leq L \leq 945a_B$) in a one–dimensional quantum dot.

The configuration of electrons in this limit is such that two of the electrons sit in the nodeless ground state and the third one in the first excited state with a node at $L/2$. This node gives a shallow minimum in the total charge density which is a characteristic of the independent electron approximation. For $L = 945a_B$, the charge density vanishes almost completely in finite regions between the three distinct peaks due to the dominant interaction effects, pointing a fully established Wigner molecule. In this quasi-classical configuration, the three electrons arrange themselves with approximately equal separation in order to minimize the electrostatic energy. Furthermore, this quasi-classical configuration is spin-independent, and thus, one can get almost degenerate (in fact very closely spaced) energy levels in the lowest ground state multiplet for the three electrons in Fig. 3.1.

The most interesting result emerged in Fig. 3.2 is the behavior of the charge density at smaller L. When $L = 1.9a_B$, the mean electron separation is of the

order of a_B, three peaks begin to appear, proving the order present in the system down to rather small L. For $L \geq 100a_B$, the peaks are well separated from each other meaning that it is the critical length for the formation of Wigner molecule. In the regime between $a_B \leq L \leq 100a_B$, the three peaks can be discernable in the total charge density and simultaneously the energy spectrum develops a multiplet structure that is characteristic of the effects of the Coulomb interaction. This multiplet structure disappears as the kinetic energy dominates the Coulombic potential energy and almost non-interacting energy spectrum can be observed for $L < a_B$ [87].

3.3 Few Electrons in a Two–Dimensional Parabolic Quantum Dot

The electron-electron interaction in quantum dots subjected to a magnetic field has been discussed in Refs. [45,85,88]. The interaction between the electrons confined in a 2D parabolic quantum dot has a dramatic effect on its energy spectrum such that physically observable ground states occur only at certain magic values of the total angular momentum, J. The expression for these magic J numbers in the spin polarized systems of 5 or less electrons is precisely given by $J = N(N-1)/2+kN$, where N is the number of electrons and k is an integer. The occurrence of energy minima at these magic J values which are all multiples of three in the three electron spin-polarized case is predicted as a direct consequence of the Pauli principle. The strength of the magnetic field determines which of the magic J value is selected. Increasing the magnetic field causes the J value of the ground state to jump from one magic value to another and hence affects the

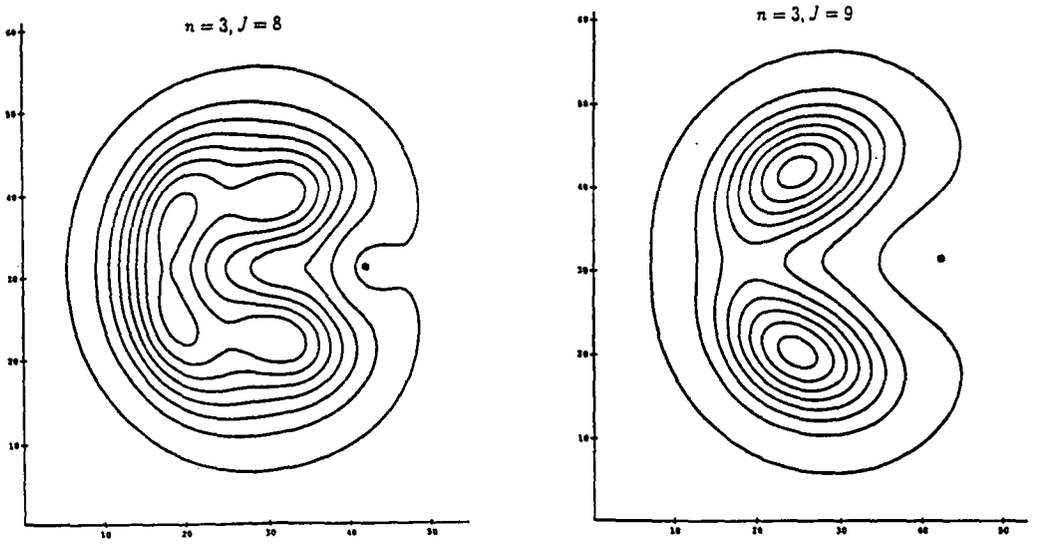

Figure 3.3: Probability distributions $P(\vec{r}, \vec{r}_o)$ for magic $J = 9$ and nonmagic $J = 8$ states of 3 interacting electrons in a two-dimensional parabolic quantum dot.

excitation spectrum. This cannot be probed by infrared spectroscopic techniques since the far-infrared radiation couples only to the center of mass motion and thus it is not sensitive to the interaction effects for the parabolic confinement potential. This makes the interaction effects difficult to observe directly. However, in [45,88], the electronic heat capacity and the magnetization are calculated to suggest that the effects of the interaction could be probed by measuring the thermodynamic properties of the electrons. Especially this is illustrated with the field dependence of the magnetization which oscillates with discontinuities when the ground state angular momentum jumps from one magic value to another.

The distinction between magic and nonmagic states can be easily seen in the probability distributions $P(\vec{r}, \vec{r}_o)$ for magic $J = 9$ and nonmagic $J = 8$ states of three interacting spin polarized electrons which is shown in Fig. 3.3. The $P(\vec{r}, \vec{r}_o)$ is defined as the probability of finding an electron at $\vec{r}$ given that there is one

at $\vec{r}_\circ$. The dot in Fig. 3.3 indicates the position of the fixed electron and $r_\circ$ is chosen to be the radius of a classical triangular Lagrangian orbit. As is seen in this figure, $P(\vec{r}, \vec{r}_\circ)$ has well separated peaks when $J = 9$, but its form is much broader than when $J = 8$. This proves the tendency for the electrons to stay apart when $J = 9$. The probability distributions for 2, 3, 4 and 5 spin polarized electrons in the limit of large angular momentum are shown in Fig. 3.4. The states are all magic states with $k = 9$ and the value of $r_\circ$ is chosen as for Fig. 3.3. It is clear that the peaks are very sharp in this limit and their positions correspond to the corners of a regular polygon. In fact, the configuration in this limit is the equilateral triangular for the three spin polarized electrons. This configuration picture suggests that the electron state in this limit is a Wigner molecule in which the equilibrium positions of the electrons are given by a classical Lagrangian orbit and whose excitations are small oscillations about this steady state orbit.

3.4 Few Electrons in a Two–Dimensional Hard–Wall Quantum Dot

The electron–electron correlations in quantum dots, mentioned above, have generally been investigated for the parabolic type confinement potential. This particular choice follows mainly from the ease of solving few–electron Schrodinger equation due to the decoupling of the center of mass and the relative coordinates. However, as also discussed in section 2.1, from the view point of the far–infrared spectroscopy, such correlation effects are hard to observe when the type of confinement potential is parabolic. In essence, what makes the theoretical study of

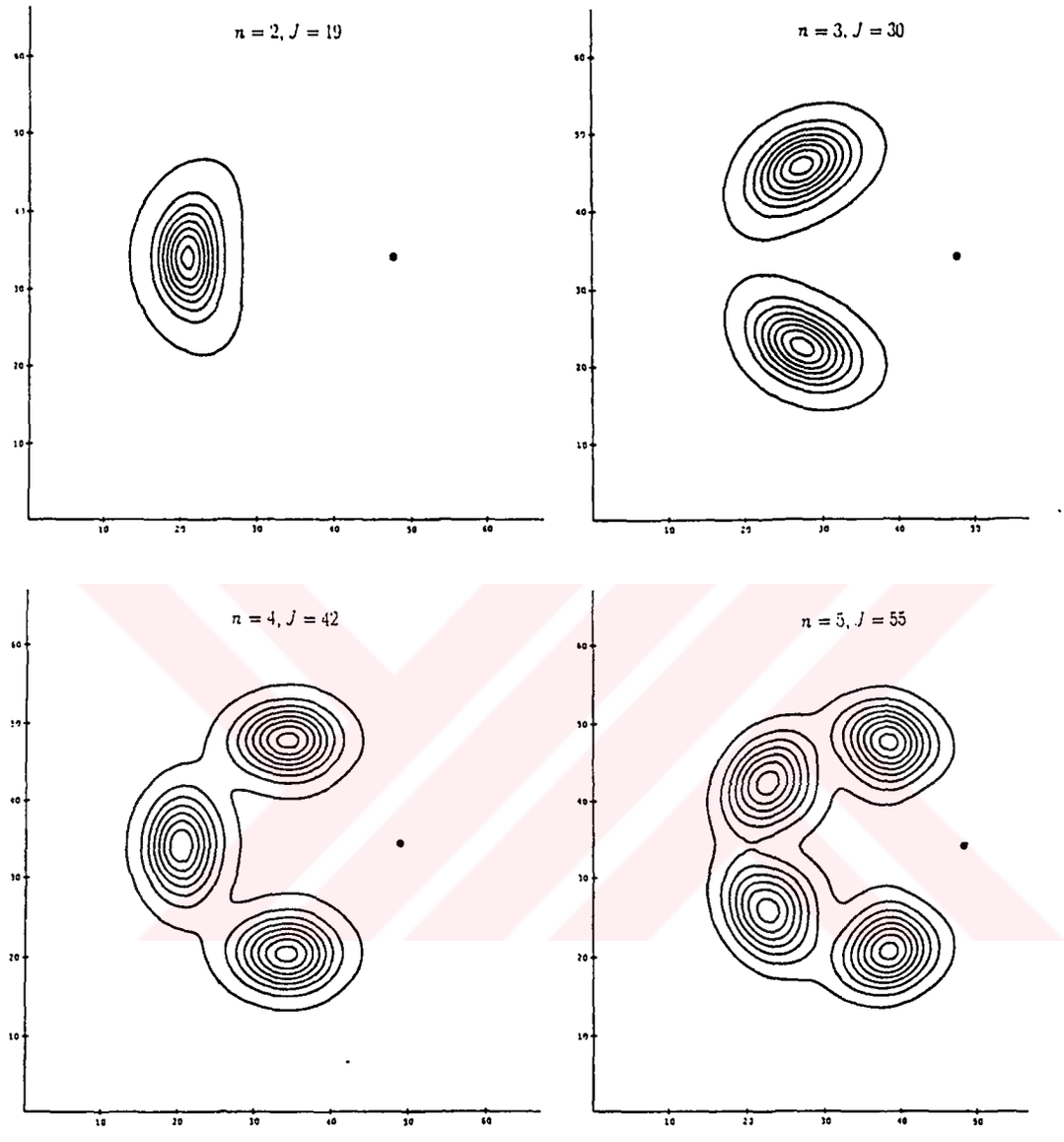

Figure 3.4: Probability distributions $P(\vec{r}, \vec{r}_o)$ for 2, 3, 4 and 5 electrons in the limit of large angular momentum.

parabolic quantum dots so common is the same thing that makes the experimental study of such systems hard. It is therefore necessary to have a coupling between the center–of–mass and the relative coordinates which eventually enables the experimentalist to probe the electronic properties of the system. For this particular reason, below we start discussing the analysis of the 2D circular quantum dot with hard–wall type confinement potential. The dot will be assumed to contain few electrons, and thus, exact diagonalization method will be used. Given the theoretical background in chapter II, it is straightforward to diagonalize the total Hamiltonian for each electron number N.

3.4.1 Energy Spectrum Results

We start by investigating the $\lambda = a/a_B$ dependence of the ground state energies for 2, 3 and 4 electrons [71]. For each electron number N, we consider certain values of the z–components of the total spin (S_z) and the total orbital angular momentum (M). They are good quantum numbers due to the circular geometry of the quantum dot. Thus, it is convenient to use certain fixed values for them when analyzing the energy spectrum of the system. In the figures below we plot the ground state energy of the dimensionless Hamiltonian $\mathcal{H}$ in (2.9) as a function of λ.

The dimensionless coupling constant λ measures the dot dimension in units of the effective Bohr radius, a_B. In our energy figures, λ covers the range from 0 to 3. In the region $0 \leq \lambda < 1$, one can analyze this problem by using the perturbation theory as was already done in Ref. [72]. However, when λ exceeds unity the

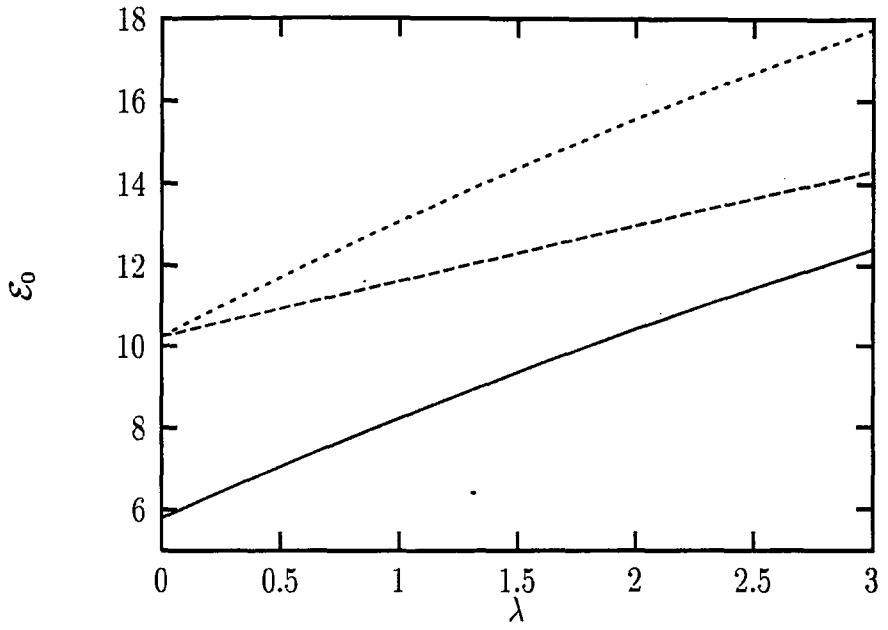

Figure 3.5: λ dependence of the ground state energy levels for two electrons.

perturbation theory does not work, and one has to resort to other techniques, such as the exact diagonalization. Hence, ground state energies will be obtained by the exact diagonalization of the dimensionless Hamiltonian in a wide range of λ.

In Fig. 3.5, λ dependence of the ground state energy for 2 electrons is presented. Here the solid curve is for $2S1$ ($M = 0$, $S_z = 0$), the dashed curve is for $2S2$ ($|M| = 1$, $S_z = 0$), and the short-dashed curve is for $2T1$ ($|M| = 1$, $S_z = 1$).

Fig. 3.6 displays the λ dependence of the ground state energy for 3 electrons. In this figure, the curves correspond to the ground state energies of $3D1$ ($|M| = 1$, $S_z = 1/2$) (solid curve), $3D3$ ($M = 0$, $S_z = 1/2$) (short-dashed curve), $3D2$ ($|M| = 2$, $S_z = 1/2$) (dashed curve), and $3Q1$ ($|M| = 0$, $S_z = 3/2$) (dotted curve).

In Fig. 3.7, we present the case of 4 electrons. The solid curve is for $4S1$

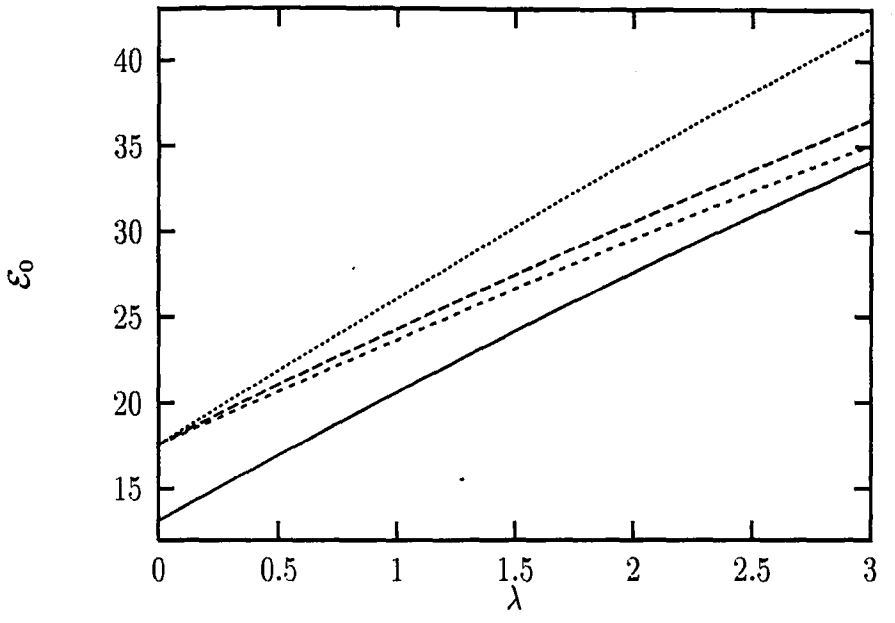

Figure 3.6: λ dependence of the ground state energy levels for three electrons.

($|M| = 2$, $S_z = 0$), the dashed curve is for $4S2$ ($M = 0$, $S_z = 0$), the short-dashed curve is for $4S3$ ($|M| = 1$, $S_z = 0$), the dotted curve is for $4T1$ ($M = 0$, $S_z = 1$), and the dot-dashed curve is for $4T2$ ($|M| = 1$, $S_z = 1$).

Our exact diagonalization results are in good agreement with those obtained from the perturbation theory [72] in the validity limits of the perturbation theory: $\lambda < 1$.

It might be interesting to compare the exact diagonalization results with those of the classical considerations. Modeling the quantum dot by an isolated conducting disc with the capacitance $C = 2\epsilon a/\pi$ one gets the classical interaction energy $E_{int.}^{class.} = 1/\lambda$, in units of $\pi\hbar^2 N^2/(4m^\star a_B^2)$, where N is the number of electrons. In Fig. 3.8, we present the λ dependence of the quantum mechanical interaction energies for $2S1$ (solid curve), $3D1$ (dashed curve) and $4S2$ (short dashed curve) in units of $\pi\hbar^2 N^2/(4m^\star a_B^2)$. The dotted curve in this figure corresponds to the

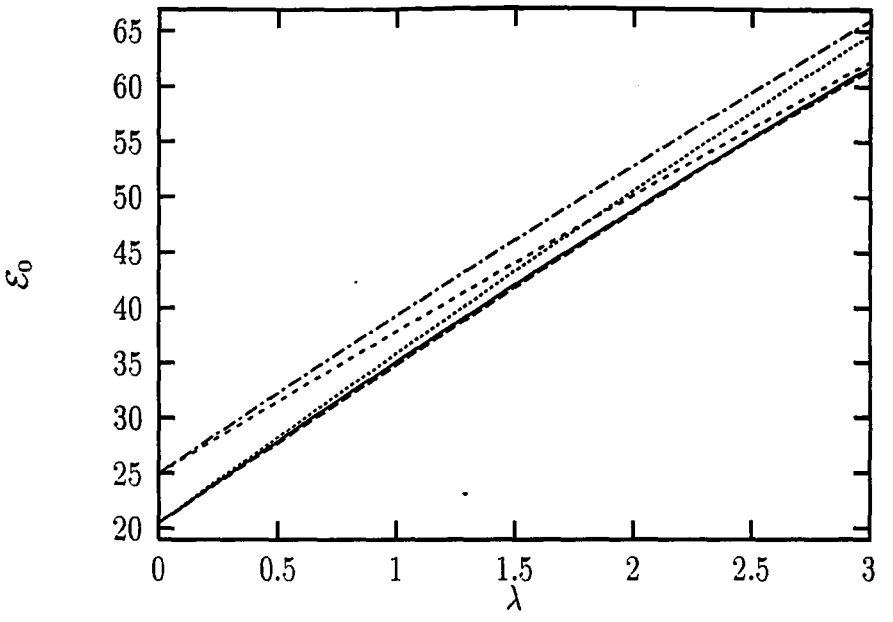

Figure 3.7: λ dependence of the ground state energy levels for four electrons.

classical interaction energy.

In fact, we see that the exact diagonalization results always remain below the classical result [72], and approach to it for large λ values, that is, for large enough dot sizes. One further observes that for small λ values, classical and quantum mechanical results behave differently, as opposed to the case of large λ. This can be attributed to the effect of electron-electron correlations, which implies that the ground state energy cannot be written as the sum of the contributions from the kinetic energy and the interaction potential [87].

Fig. 3.9 shows the dependence of the dimensionless ground state energy per particle, $\mathcal{E}_0/N$, on the particle number N for different λ values. For small λ values, $\mathcal{E}_0/N$ deviates from a linear behavior due to the dominance of the free Hamiltonian. On the other hand, when the interaction potential becomes dominant with increasing λ value, the formation of an inhomogeneous charge density

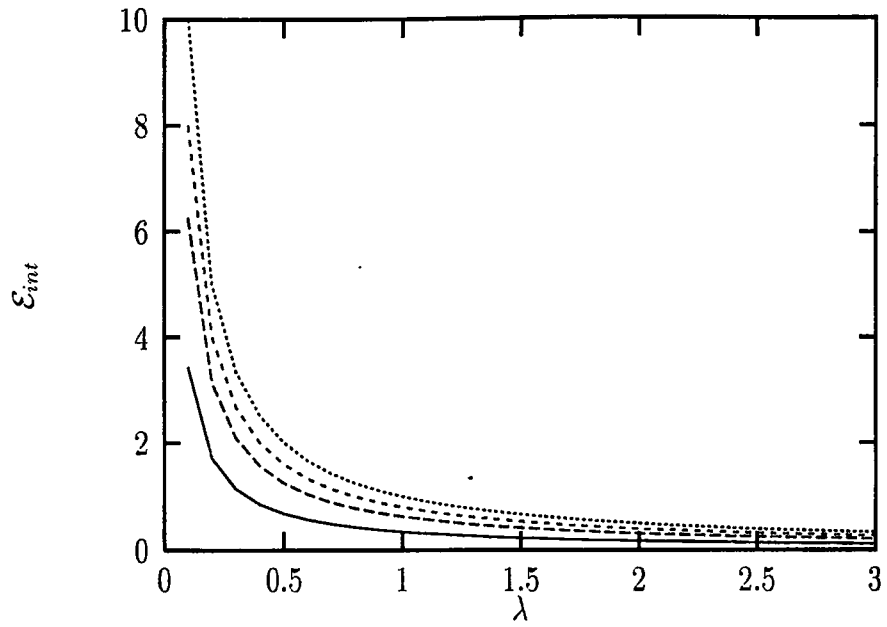

Figure 3.8: Comparison of the classical interaction energy with the lowest three quantum mechanical interaction energies

(Wigner molecule) prevents $\mathcal{E}_0/N$ to change linearly with N.

3.4.2 Charge Density and The Pair Correlation Function Results: The Wigner Molecule

So far we have mainly analyzed the λ–dependence of the ground state energy for given N, M and S_z values. The figures in the previous section establish the energy spectrum of the system, and almost agree with the perturbation theory results. Now we turn to detailed discussion of the electron–electron correlations in the same structure, that is, a 2D circular quantum dot with the hard–wall type confinement potential. In what follows we assume three spin polarized electrons with vanishing total orbital angular momentum, $M = 0$. Using the analytical derivations of chapter II with $S_z = 3/2$ and $M = 0$, we investigate the size and peripheric dependencies of the charge density and the pair correlation function

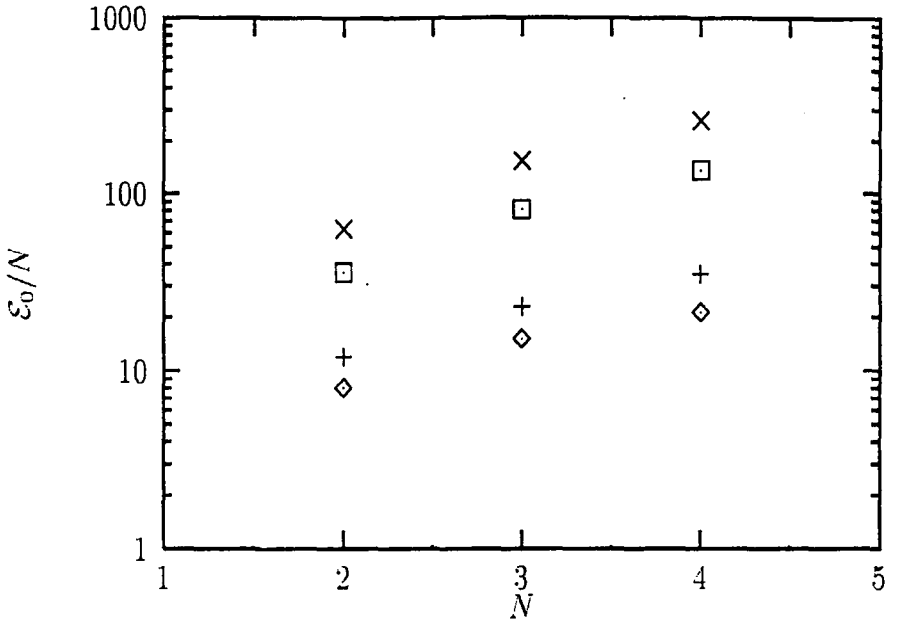

Figure 3.9: Dimensionless ground state energies per particle $\mathcal{E}_0/N$ versus the particle number N for $\lambda = 5(\diamond)$, $\lambda = 10(+)$, $\lambda = 50(\square)$, $\lambda = 100(\times)$

for three electrons [89].

In contrast to the parabolic confinement potential, one cannot find an analytic expression for r_0, the radial distance minimizing the total potential energy, for the hard-wall type confinement potential. Despite of this, for large enough λ values, the three electrons are expected to locate at the vertices of an equilateral triangle with side length r_0 which occurs at some distance in the radial direction. This favorable structure will be an indication of the minimum energy configuration of the electrons. These features will be checked out by an explicit numerical study described below.

The r and λ dependencies of the charge density $\rho(\vec{x})$ (normalized to N=3 for each λ) for the state $|S_z = 3/2, M = 0 >$ is shown in Fig. 3.10. The three curves in this figure describe the variations of the electron distribution as a function of λ and r. For small λ (e. g. $\lambda = 1$), electrons have a non-negligible

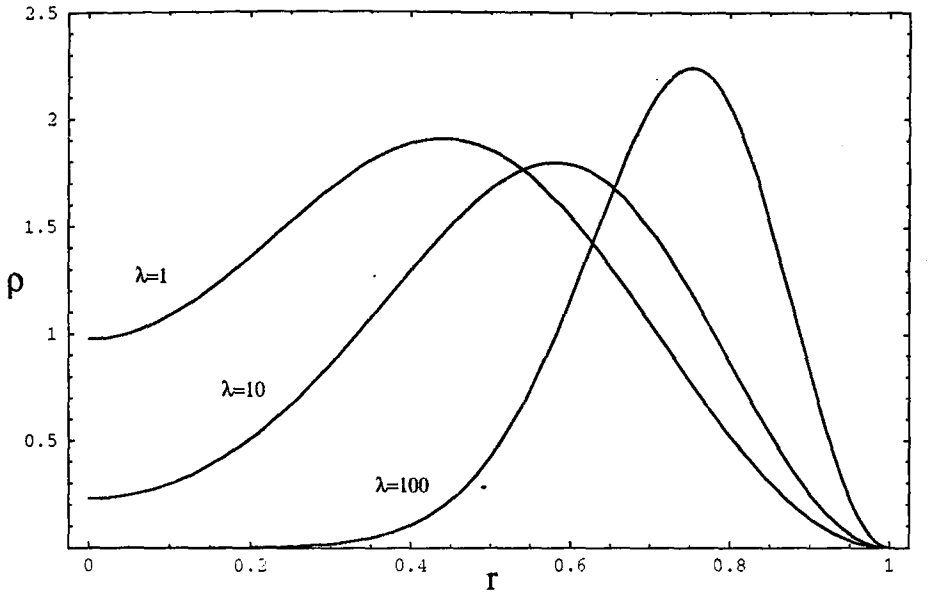

Figure 3.10: Variation of the charge density $\rho(\vec{x})$ with radial distance r and the dot size λ.

distribution at the center of the dot though the maximum is reached away from the origin. This behavior of $\rho(\vec{x})$ shows that for small λ, $J_{m=0}(r)$ is the dominant component, especially around small r, in the Bessel expansion given in chapter II. As λ increases, however, the charge density vanishes gradually around the center of the dot (e. g. $\lambda = 10, 100$). In this limit, one observes the dominance of the $J_{m>0}$; because they vanish at the origin by the definition. Besides the behavior of the charge density close to the center of the dot, one also observes that the higher the λ, the sharper the peaks. The sharper peaks show the most probable radial position of the electrons. Additionally, as λ increases, the electrons get shifted towards the edge of the dot, but they never reach there because of the infinite potential barrier. For example for $\lambda = 100$, the electrons are distributed most probably along the periphery of the circle whose radius is $r \sim 0.7$ within the quantum dot. This result follows from the fact that the system minimizes

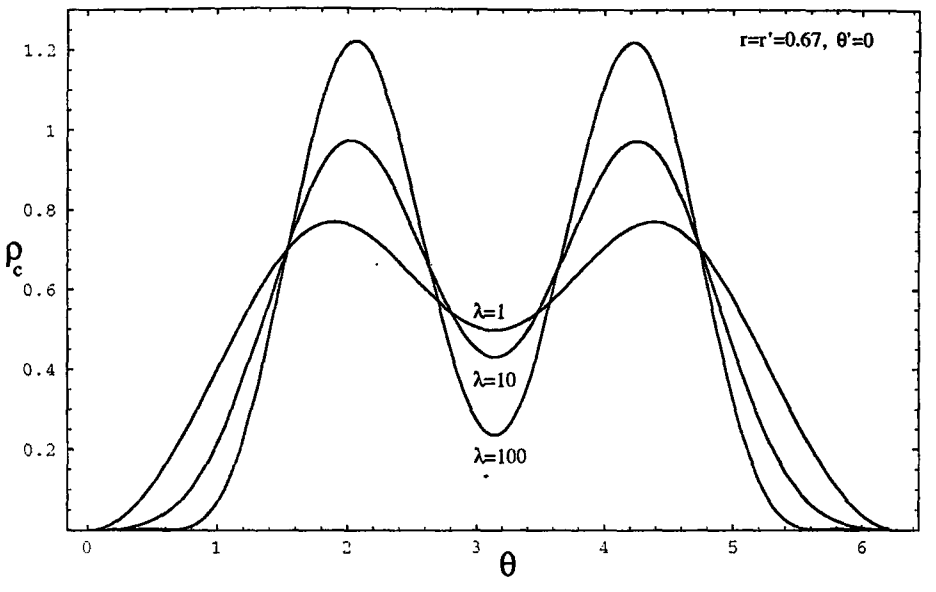

Figure 3.11: Variation of the pair correlation function with θ and λ for $r = r' = 0.67$ and $\theta' = 0$.

its electrostatic energy which is the dominant part of the total Hamiltonian for large enough λ values. The behavior of the charge density informs us only about the radial distribution of electrons. Therefore, to have a complete knowledge of the planar electron–electron correlations, we must also investigate the variation of the pair correlation function $\rho_c(\vec{x}, \vec{x}')$ with r, θ as well as λ.

In Fig. 3.11, the variation of the pair correlation function normalized to N(N-1)=6 with θ and λ for $r = r' = 0.67$ and $\theta' = 0$ is presented. The pair correlation function $\rho_c(\vec{x}, \vec{x}')$ is the probability distribution of $N - 1$ electrons when one of N electrons is located at $\vec{x}'$. In the case of three electrons, the pair correlation function, in Fig. 3.11, shows the angular distribution of two electrons within the circular quantum dot. The fact that the pair correlation function has always two distinct peaks and vanishes at $\theta = 0$, as is seen in this figure, the Pauli exclusion principle is satisfied as expected.

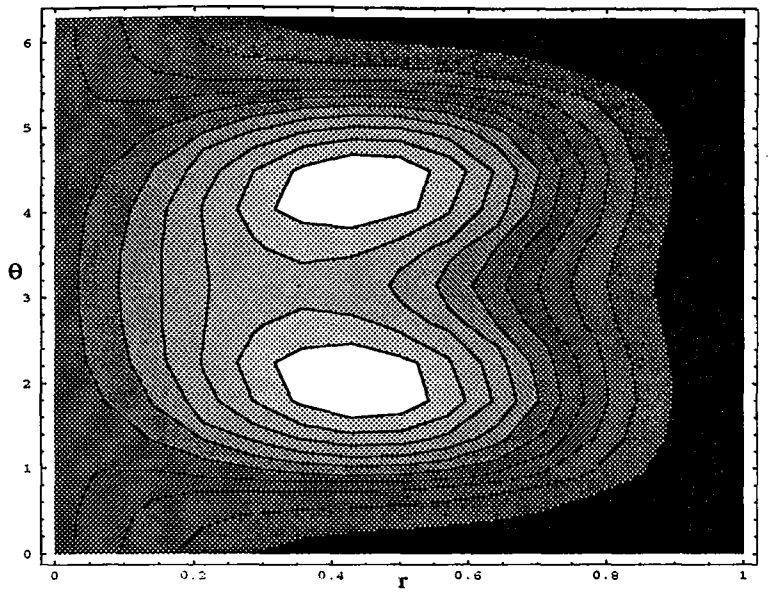

Figure 3.12: Contour lines showing the pair correlation function on the $(r-\theta)$ plane for $r'=0.67$, $\theta'=0$, and $\lambda=1$.

An important property of the pair correlation function follows from its variation with the dot size in units of the effective Bohr radius. One notices that for small λ values, peaks are not sharp and electrons do not have a well-defined configuration. Namely, the pair correlation function is not diminished significantly between the two peaks. The small λ limit shows nothing but the atomic regime of confinement where the dot size is of the order of effective Bohr radius or smaller; and their average kinetic energy exceeds the Coulombic repulsion. In this limit, it is well known that the electrons are completely delocalized in the quantum dot. That is, they do not possess well–defined positions in the plane of the dot. It is also known that the perturbation theory is a reliable tool to investigate the physical properties of the dot [72] for the values of $\lambda < 1$. Indeed, the Hartree-Fock method can be applied to the dot structures just as in the few-electron natural atoms [43].

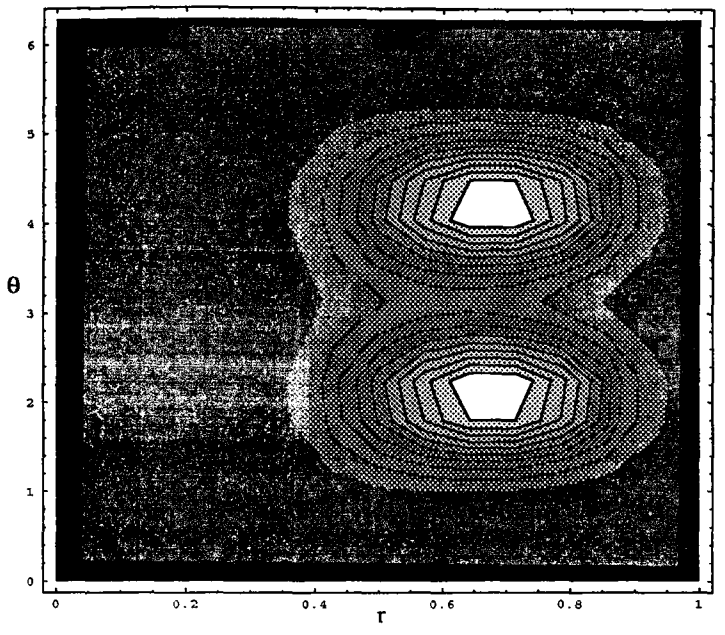

Figure 3.13: The same as in Fig. 3.12 but for $\lambda = 100$.

The Fig. 3.11 shows clearly that the peaks get sharper with increasing λ and the pair correlation function assumes gradually two distinct peaks between which there is a strong depletion. Therefore, the higher the dot size, the smaller the overlap between the two peaks. As λ increases, the peaks approach to fixed positions such that their angular separation is $\sim 120°$. This angular separation constitutes an equilateral triangular structure as observed in 2D parabolic quantum dots [43,74]. This geometrical rearrangement corresponds to the minimum energy configuration of the system where its kinetic energy is smaller than the Coulomb energy. The latter is minimized by the equilateral triangular configuration of the electrons. The approach to this configuration for large dot sizes is nothing but the formation of the well-known Wigner molecule structure which has been shown to exist in other types of dots too [43,75]. As a result, for large dot sizes the electrons locate at fixed positions in the dot by minimizing their

electrostatic energy.

For a better understanding of the behavior of the electron distribution in the dot, it may be convenient to analyze the pair correlation function in the $r-\theta$ plane in which both radial and angular variations become visible. Fig. 3.12 shows the contour lines of $\rho_c(\vec{x},\vec{x}')$ in the $r-\theta$ plane for $\theta'=0$, $r'=0.67$, and $\lambda=1$. In accordance with Fig. 3.10 and Fig. 3.11, there is a non-negligible correlation between the electrons for small r; also the maxima are reached away from the origin, $r\sim 0.4$. Moreover, near the edge of the dot, the correlation distribution is highly suppressed. One further notices that the pair correlation function in between the two peaks is not suppressed at all.

To illustrate the effects of larger dot sizes on Fig. 3.12, the pair correlation function in the $r-\theta$ plane is shown in Fig. 3.13 for $\lambda=100$. As is seen, there are important differences between Fig. 3.12 and Fig. 3.13. First of all, the peaks are shifted towards the edge of the dot in comparison with Fig. 3.10. Next, the peaks are now sharpened and the pair correlation between them is reduced significantly. In this sense, the differences between these two figures prove the formation of the Wigner molecule of the electrons with increasing Coulombic repulsion among them with ever growing λ.

CHAPTER 4

CONCLUSIONS

4.1 Contributions

Quantum dot structure is the ultimate limit of the low dimensional quantum systems. These structures exhibit not only many of the quantum phenomena which are naturally appearing in real atoms, but also new physics (also quantum in origin) which has no analogue in real atoms. These novel effects influence strongly their electrical properties. Such effects mainly arise from the interactions between the electrons. In this study, we have concentrated on a two dimensional circular quantum dot and obtained its energy spectrum for 2, 3 and 4 electrons using the exact diagonalization method. Type of confining potential for this circular dot was chosen to be the hard-wall type to obtain observable effects of the electron-electron interactions on the energy spectrum via the coupling of the center-of-mass and the relative coordinates. We investigated the coupling constant ($\lambda = a/a_B$) dependence of the ground state energy for each electron number for the given values of the good quantum numbers: the total spin, and the z–components of the total spin and the total orbital angular momentum. Our exact diagonalization results are in very good agreement with those obtained from the perturbation method for $\lambda \leq 1$. Since the perturbation theory is not applicable

for λ values exceeding unity, the exact diagonalization method is commonly most preferred one especially for small number of electrons and large dot sizes ($\lambda \geq 1$). Apart from the perturbative considerations, we also compare the quantum mechanical interaction energies with that of the classical consideration. Indeed, it is observed that the exact diagonalization results are below the classical prediction, and approach to it for large λ values, or equivalently, large enough dot sizes. In addition, for small λ values or equivalently small dot sizes, classical and quantum mechanical results behave different due to the enhancement of the quantum effects. We also investigate the dependence of the dimensionless ground state energy per particle, $\mathcal{E}_0/N$, on the particle number N for different λ values. For small λ values, $\mathcal{E}_0/N$ deviates from a linear behavior due to the dominance of the free Hamiltonian. On the other hand, when the interaction potential becomes dominant with increasing λ value, the formation of an inhomogeneous charge density (Wigner molecule) prevents $\mathcal{E}_0/N$ to change linearly with N.

In the next step, we investigate the effects of the electron-electron interactions on the charge density and the pair correlation functions for three spin polarized electrons. From the variation of the charge density with the radial distance r and the dot size λ, one can observe that for small dot sizes electrons have non-negligible distribution at the center of the dot though the maximum is reached away from the origin. As the dot size increases, the charge density vanishes gradually around the center of the dot and the electrons get shifted towards its edge, but never reaching there because of the infinite potential barrier. The sharper peaks show the most probable radial position of the electrons. This

result follows from the fact that electrons minimize their electrostatic energy which is the dominant component in the total Hamiltonian for large dot sizes. For vanishing total orbital angular momentum, the behavior of the charge density gives information only on the radial distribution of the electrons. Thus, to form an opinion about the planar electron–electron correlations, we study the pair correlation function with radial distance r, azimuthal angle θ and the dot size λ. From the angular distribution of two electrons, while the third one is located at a fixed point within the dot, for small λ values the peaks are not sharp and electrons do not have a well-defined configuration. That is, the pair correlation function is not diminished significantly between the two peaks. This small λ limit shows the atomic regime of the confinement where the average kinetic energy exceeds the Coulombic repulsion. In this limit, the Hartree-Fock approximation can be applied just as in the few-electron real atoms to investigate the physical properties of the dot. When λ is increased, the peaks get sharper and the pair correlation function gradually assumes two distinct peaks between which there is a strong depletion. In fact, as λ increases the peaks approach to fixed positions such that their angular separation is $\sim 120°$. This angular separation constitutes an equilateral triangular structure which corresponds to the minimum energy configuration of the electrons. The approach of the configuration to an equilateral triangular structure for large dot sizes indicates the formation of the Wigner molecule in which electrons assume fixed positions in the dot by minimizing the dominant electrostatic energy.

We also study the pair correlation function in the $r - \theta$ plane for a better

understanding of the behavior of the electron distribution in the dot for small and large λ values. From the contour lines of the pair correlation function for small λ value, we observe that there is a non-negligible correlation between the electrons for small r and that the maxima are reached away from the origin. Moreover, while the correlation distribution is highly suppressed near the edge of the dot, it is not suppressed in between the two peaks at all. We finally illustrate the effects of larger dot sizes (large λ) to the pair correlation function in the $r-\theta$ plane. In the large λ limit, the peaks are sharpened and shifted towards the edge of the dot. Furthermore, the pair correlation between the two peaks is seen to be reduced significantly, pointing out the formation of the Wigner molecule with ever growing λ.

4.2 Future Prospects

The research on single quantum dots, both experimental and theoretical, to understand their physical properties is very important and useful for the future device applications. Since a quantum dot is an intermediate structure between a bulk system and a real atom, it is assumed to be an ideal object for the fundamental studies of many particle systems and electron-electron interactions. By changing the size of the quantum dot, one can transform the quantum mechanical system of weakly interacting particles into a strongly correlated quasiclassical system which shows properties analogues to Wigner crystallization. If a quantum dot is not too small, then it proposes to study the both the Wigner lattice and the transition from the Wigner regime to the independent electron regime as the

electron density is increased. The fundamental difference between the Wigner regime in a few electron quantum dot and the infinite Wigner lattice is the effect of the boundaries that can increase the ground state spin to the values larger than $S = 0$ or $S = 1/2$. In this work only the three spin polarized electrons are discussed to understand their distributions within a 2D circular quantum dot with the varying dot size. In the continuation of this work, one may study more electrons confined in a different type of dot geometry and investigate their distributions as the dot size is changed. Especially, the configuration of these electrons when they form the Wigner molecule may be a very interesting research subject.

At this point it is convenient to discuss another important case. Very recently Egger et. al. [90] have studied the crossover from the Fermi liquid to the Wigner molecule regime for a parabolic quantum dot for up to eight electrons. They have used the quantum Monte Carlo method to evaluate the electron energy levels as well as the electron–electron correlation function. They report that the transition from the free electron regime to the Wigner molecule occurs at the dimensionless density parameter $r_s \sim 4$ regardless of the number of electrons. Here we expect that this crossover point should depend on the details of the confinement potential. Therefore, the question whether such a universal transition point also exists in the hard-wall quantum dots is presently an open problem.

REFERENCES

[1] A. I. Ekimov and A. A. Onushchenko, JETP Letter **34**, 345 (1981).

[2] A. I. Ekimov and A. A. Onushchenko, JETP Letter **40**, 1136 (1984).

[3] A. I. Ekimov, Al. L. Efros, and A. A. Onushchenko, Solid State Communications **56**, 921 (1985).

[4] J. Warnock and D. D. Awschalom, Physical Review **B32**, 5529 (1985).

[5] J. Warnock and D. D. Awschalom, Applied Physics Letter **48**, 425 (1986).

[6] Li-Chi Liu and S. H. Risbud, Journal of Applied Physics **68**, 28 (1990).

[7] R. Rossetti, J. L. Ellison, J. M. Gibson, and L. E. Brus , Journal of Chemical Physics **80**, 4464 (1984).

[8] L. Brus, Journal of Physical Chemistry **90**, 2555 (1986).

[9] A. P. Alivisatos, T. D. Harris, L. E. Brus, and A. Jayaraman, Journal of Chemical Physics **89**, 5970 (1988).

[10] M. L. Steigerwald, A. P. Alivisatos, J. M. Gibson, T. D. Harris, R. Kortan, A. J. Muller, A. M. Thayer, T. M. Duncan, D. C. Douglass, and L. E. Brus, Journal of American Chemical Society **110**, 3046 (1988).

[11] M. L. Steigerwald and L. E. Brus, Accounts of Chemical Research **23**, 183 (1990).

[12] L. Brus, Journal of Physical Chemistry **95**, 1572 (1991).

[13] Y. Wang and N. Herron, Journal of Physical Chemistry **91**, 257 (1987).

[14] J. N. Randall, M. A. Reed, T. M. Moore, R. J. Matyi, and J. W. Lee, Journal of Vacuum Science and Technology **B6**, 302 (1988).

[15] M. A. Reed, J. N. Randall, R. J. Aggarwal, R. J. Matyi, T. M. Moore, and A. E. Wetsel, Physical Review Letters **60**, 535 (1988).

[16] U. Meirav, P. L. McEuen, M. A. Kastner, E. B. Foxman, A. Kumar, and S. J. Wind, Zeitschrift fur Physik **B85**, 357 (1991).

[17] T. J. Thornton, M. Pepper, H. Ahmed, D. Andrews, and G. J. Davies, Physical Review Letters **56**, 1198 (1986).

[18] L. P. Kouwenhoven, N. C. van der Vaart, A. T. Johnson, W. Kool, C. J. P. M. Harmans, J. G. Williamson, A. A. M. Staring, and C. T. Foxon, Zeitschrift fur Physik **B85**, 367 (1991).

[19] B. J. van Wees, L. P. Kouwenhoven, J. R. Kraayeveld, F. W. J. Hekking, and C. J. P. M. Harmans, Physica **B165**, 847 (1990).

[20] L. P. Kouwenhoven, F. W. J. Hekking, B. J. van Wees, C. J. P. M. Harmans, C. E. Timmering, and C. T. Foxon, Physical Review Letters **65**, 361 (1990).

[21] J. F. Carlin, R. Houdre, A. Rudra, and M. Ilegems, Applied Physics Letters **59**, 3018 (1991).

[22] J. Ahopelto, A. Yamaguchi, K. Nishi, A. Usui, and H. Sakaki, Japanese Journal of Applied Physics **32**, L32 (1993).

[23] C. M. Reaves, V. Bressler-Hill, M. Krishnamurthy, S. Verma, P. M. Petroff, W. H. Weinberg, and S. P. DenBaars, Abstract of the IEEE VI International Conference of InP and Related Materials, Santa Barbara (1994).

[24] S. Fafard, Z. Wasilewski, J. McCaffrey, S. Raymond, and S. Charbonneau, Applied Physics Letters **68**, 991 (1996).

[25] B. R. Bennett, R. Magno, and B. V. Shanabrook, Applied Physics Letters **68**, 505 (1996).

[26] F. Hatami et al, Applied Physics Letters **67**, 656 (1995).

[27] C. K. Sun, G. Wang, J. E. Bowers, B. Brar, H. R. Blank, H. Kroemer, and M. H. Pilkuhn, Applied Physics Letters **68**, 1543 (1996).

[28] D. J. Eaglesham and M. Cerullo, Physical Review Letters **64**, 1943 (1990).

[29] J. Tersoff and F. K. LeGoues, Physical Review Letters **72**, 3570 (1994).

[30] J. Tersoff, C. Teichert, and M. G. Lagally, Physical Review Letters **76**, 1675 (1996).

[31] L. Goldstein, F. Glas, J. Y. Marzin, M. N. Charasse, and G. Roux, Applied Physics Letters **47**, 1099 (1985).

[32] C. W. Snyder, B. G. Orr, D. Kessler, and L. M. Sander, Physical Review Letters **66**, 3032 (1991).

[33] D. Leonard, M. Krishnamurthy, C. M. Reaves, S. P. DenBaars, and P. M. Petroff, Applied Physics Letters **63**, 3203 (1993).

[34] J. Oshinowo, M. Nishioka, S. Ishida, and Y. Arakawa, Applied Physics Letters **65**, 1421 (1994).

[35] J. M. Gerard, J. B. Genin, J. Lefebvre, J. M. Lebouche, and F. Barthe, Journal of Crystal Growth **150**, 351 (1995).

[36] D. V. Averin and K. K. Likharev, in Mesoscopic Phenomena in Solids, B. L. Altshuler, P. A. Lee, R. A. Webb, editors, Elsevier, Amsterdam, p. 173 (1991).

[37] H. van Houton and C. W. J. Beenakker, Physical Review Letters **63**, 1893 (1989).

[38] G. W. Bryant, Physical Review Letters **59**, 1140 (1987).

[39] Ch. Sikorski and U. Merkt, Physical Review Letters **62**, 2164 (1989).

[40] Ch. Sikorski and U. Merkt, Physical Review Letters **64**, 3100 (1990).

[41] Ch. Sikorski and U. Merkt, Surface Science **229**, 282 (1990).

[42] B. Meurer, D. Heitmann and K. Ploog, Physical Review Letters **68**, 1371 (1992).

[43] J. H. Jefferson, W. Haeusler and D. Malvern, Molecular Physics Reports **17**, 81 (1997).

[44] M. Kastner, Physics Today **January**, 24 (1993).

[45] P. A. Maksym and T. Chakraborty, Physical Review Letters **65**, 108 (1990).

[46] D. Pfannkuche and R. R. Gerhardts, Physical Review **B44**, 13132 (1991).

[47] V. Gudmundsson and R. R. Gerhardts, Physical Review **B43**, 12098 (1991).

[48] Z. L. Ye and E. Zaremba, Physical Review **B50**, 17217 (1994).

[49] F. M. Peeters and V. A. Schweigert, Physical Review **B53**, 1468 (1996).

[50] A. Brataas, U. Hanke and K. A. Chao, Semiconductor Science and Technology **12**, 825 (1997).

[51] A. Lorke, J. P. Kottaus and K. Ploog, Physical Review Letters **64**, 2559 (1990).

[52] B. Meurer, D. Heitmann and K. Ploog, Physical Review **B48**, 11488 (1993).

[53] R. Strenz et al, Physical Review Letters **73**, 3022 (1994).

[54] U. Meirav, M. A. Kastner and S. J. Wind, Physical Review Letters **65**, 771 (1990).

[55] M. A. Kastner, Reviews of Modern Physics **64**, 849 (1992).

[56] T. Demel, D. Heitmann, P. Grambow and K. Ploog, Physical Review Letters **64**, 788 (1990).

[57] P. L. McEuen et al, Physical Review **B45**, 11419 (1992).

[58] R. C. Ashoori et al, Physical Review Letters **68**, 3088 (1992).

[59] A. T. Johnson et al, Physical Review Letters **69**, 1592 (1992).

[60] J. Weis, R. J. Haug, K. Klitzing and K. Ploog, Physical Review Letters **71**, 4019 (1993).

[61] U. Merkt, J. Huser and M. Wagner, Physical Review **B43**, 7320 (1991).

[62] M. Wagner, U. Merkt and V. Chaplik, Physical Review **B45**, 1951 (1992).

[63] J. S. De Groote and J. E. Hornos, Physical Review **B46**, 12773 (1992).

[64] D. Pfannkuche, V. Gudmundsson and P. A. Maksym, Physical Review **B47**, 2244 (1993).

[65] T. Brandes, W. Haeusler, K. Jaurequi, B. Kramer and D. Weinmann, Physica **B189**, 16 (1993).

[66] X. C. Xie, S. Das Sarma and S. He, Physical Review **B48**, 8454 (1993).

[67] L. Wang, J. K. Ahang and A. R. Bishop, Physical Review Letters **73**, 585 (1994).

[68] A. H. Guerrero, Semiconductor Science and Technology **10**, 759 (1995).

[69] E. A. Hylleraas, Zeitschrift fur Physik **54**, 347 (1929).

[70] D. Babic, R. Tsu and R. F. Greene, Physical Review **B45**, 14150 (1992).

[71] N. Akman and M. Tomak, Physica **B262**, 317 (1999).

[72] J. O. Fjarestad, A. Matulis and K. A. Chao, Physica Scripta **T69**, 138 (1997).

[73] A. Matulis, J. O. Fjarestad and K. A. Chao, Physica Scripta **T69**, 85 (1997).

[74] X.-G. Li, W.-Y. Ruan, C.-G. Bao and Y.-Y. Liu, Few Body Systems **22**, 91 (1997).

[75] K. Jauregui, W. Haeusler and B. Kramer, Europhysics Letters **24**, 581 (1993).

[76] L. D. Landau, Soviet Physics JETP **35**, 70 (1959).

[77] E. P. Wigner, Physical Review **46**, 1002 (1934).

[78] M. Gell-Mann and K. A. Brueckner, Physical Review **106**, 364 (1957).

[79] I. Shavitt, B. Ross and B. O. Siegbahn, in Modern Theoretical Chemistry, Vol. 3, edited by H. F. Schaefer, (Plenum, New York, 1977), p. 189.

[80] S. Wilson, in Theoretical Chemistry, Vol. 4, (Royal Society of Chemistry, London, 1981), p. 1.

[81] D. M. Ceperley and B. J. Alder, Physical Review Letters **45**, 566 (1980).

[82] B. Tanatar and D. M. Ceperley, Physical Review **B39**, 5005 (1988).

[83] V. B. Timofeev, in Optical Properties of Semiconductors, edited by G. Martinez, ASI, Kluwer Academic Publishers, 1993.

[84] R. G. Clark, Physica Scripta **T39**, 45 (1991).

[85] P. A. Maksym, Physica **B184**, 385 (1993).

[86] P. Hawrylak and D. Pfannkuche, Physical Review Letters **70**, 485 (1993).

[87] W. Haeusler and B. Kramer, Physical Review **B47**, 16353 (1993).

[88] P. A. Maksym and T. Chakraborty, Physical Review **B45**, 1947 (1992).

[89] N. Akman and M. Tomak, Physica **E4**, 277 (1999).

[90] R. Egger, W. Haeusler, C. H. Mak and H. Grabert, Physical Review Letters **82**, 3320 (1999).

VITA

Nurten Akman was born in Ankara on October 16, 1969. She received her B.S degree from the Department of Physics of the Middle East Technical University in Ankara, in 1991. In August 1994, she received her M.S degree in the field of experimental condensed matter physics from the same department. After 1994, she continued her Ph.D study under the supervision of Prof. Mehmet Tomak on the electron-electron interactions in two dimensional quantum dots. Her research has been published in the international refereed journals Semiconductor Science and Technology, Physica B, and Physica E.